Multistage spatial model for informing release of *Wolbachia*-infected mosquitoes as disease control

Zhuolin Qu[1*], Tong Wu[1]

1 Department of Mathematics, University of Texas at San Antonio, San Antonio, TX, United States of America

* Corresponding author
Email: zhuolin.qu@utsa.edu

Abstract

Wolbachia is a naturally occurring bacterium that can infect *Aedes* mosquitoes and reduce the transmission of diseases such as dengue fever, Zika, and chikungunya. Field trials worldwide have explored its potential for epidemic control. We introduce a partial differential equation model to simulate the spatial spread of *Wolbachia* infection in mosquito populations. The model incorporates detailed mosquito life stages, intricate *Wolbachia* maternal transmission, and two-dimensional mosquito dispersion. Building on prior studies showing a threshold of infected mosquitoes is required for persistence, we identify a spatial threshold, termed the "critical bubble", for achieving self-sustaining Wolbachia infection. When releasing beyond this threshold, the model predicts a spatial wave of *Wolbachia* infection. We quantify how the threshold and infection wave velocity depend on the diffusion process and ecological parameters, and examine different intervention scenarios to inform efficient *Wolbachia* release strategies. Our results suggest that: (1) pre-release mitigations targeting adult mosquitoes more effectively reduces the threshold than targeting aquatic stages; (2) releases in the dry regions lower the threshold, but the infection wave propagation may slow down or stall at the dry-wet interfaces due to the heterogeneity in carrying capacities; and (3) initiating releases just before the wet season reduces the release threshold.

Keywords

Wolbachia-based control; reaction-diffusion model; spatial dynamics; threshold; population replacement

1 Introduction

Mosquitoes are among the deadliest creatures in the world due to the diseases they transmit. Traditional control strategies, such as larvicides and indoor residual spraying, aim to reduce mosquito populations. However, these methods often face challenges related to sustainability, resistance, and implementation logistics [1].

Novel biological controls are being developed to provide alternative strategies for managing mosquito populations and the spread of diseases. These include *Wolbachia*-based methods, which can be used for either population suppression [2, 3] or replacement [4], as well as the sterile insect technique [5, 6] and gene editing [7, 8]. Among these approaches, *Wolbachia*-based controls have shown promise in field trials for *Aedes* mosquitoes to combat dengue epidemics worldwide [9–12]. Extensive laboratory work has also been conducted to introduce *Wolbachia* into *Anopheles* mosquitoes as a potential malaria control strategy [13–15].

The *Wolbachia*-based population replacement strategy aims to replace the wild-type mosquitoes with *Wolbachia*-infected ones by leveraging their reproductive advantages, achieved through a mechanism called cytoplasmic incompatibility (CI) [2]. Moreover, unlike wild-type mosquitoes, *Wolbachia*-infected mosquitoes are less capable of transmitting diseases [4]. A key aspect of this population replacement approach is the existence of a threshold infection frequency: if the initial proportion of infected mosquitoes exceeds this threshold, *Wolbachia* can persist and spread through the population; otherwise, the infection will eventually be lost. This has been observed in both population cage experiments [16] and field trials [17]. Identifying and understanding this threshold is critical for designing effective field release programmes.

Mathematical models have played an essential role in characterising this threshold and informing field trials. Numerous ordinary differential equation (ODE) models have been developed to capture the dynamics of *Wolbachia* invasion under various biological assumptions (e.g., [18–25]). In these models, the invasion threshold emerges from a balance between the fitness costs of *Wolbachia* infection (reduced lifespan and fecundity in female mosquitoes) and the reproduction advantage conferred by the CI effect of the *Wolbachia*-infection. Mathematical characterisations of this threshold typically reveal backward bifurcation [18, 19, 21, 25, 26]. However, the threshold derived from ODE models may not accurately capture the dynamics of *Wolbachia* invasion in field releases, as they typically overlook the spatial structure, such as localised releases, mosquito dispersal, and patch-wise variation in habitat availability.

A range of modelling frameworks has been used to incorporate the spatial processes at different biological and spatial scales. Patch or metapopulation models represent landscapes as networks of discrete habitats with movement between them. This approach can capture fragmented landscapes and has been used to explore *Wolbachia* invasion under spatially structured mosquito populations [27–29]. Agent-based models (ABMs) provide an alternative, high-resolution approach in which individual mosquitoes move and interact according to rules informed by empirical data. ABMs have been applied to modelling mosquito-borne disease transmission and other vector control, such as gene-drive interventions [30–33]. These models can incorporate fine-scale environmental heterogeneity and movement behaviour, but they are more computationally intensive, require detailed parametrisation, and often lack analytical tractability.

Reaction-diffusion partial differential equation (PDE) models provide a middle ground between biological realism and analytical structure. Barton and Turelli [34] introduced a one-PDE reaction-diffusion model incorporating the *Wolbachia*-induced CI effect and fitness costs. Their model used a cubic approximation for maternal transmission of *Wolbachia* and tracked the fraction of infection among the mosquitoes. The model was later extended to include biologically realistic non-Gaussian dispersal kernels [23], which account for a higher probability of long-distance mosquito flights. Both models identified a minimal *Wolbachia*-infection area as a threshold for *Wolbachia* establishment. Similar frameworks have been applied to account for imperfect maternal transmission [35]. Huang et al. [36] developed a two-PDE model to track infected and uninfected mosquito cohorts separately, and their analyses indicate that spatial diffusion slightly increases the threshold. Duprez et al. [37] formulated a two-PDE model, which was then reduced to a one-PDE model for an optimal control problem to determine the best spatial strategy for *Wolbachia* release.

While these spatial models have yielded valuable insights, many simplify mosquito biology by omitting aquatic stages or male mosquitoes, which may limit their ability to evaluate integrated interventions such as larval control or pre-release mitigation. Moreover, many assume homogeneous environments, which restricts their applicability to inform field settings where resource availability, climate, and population density vary across space and time.

In this study, we develop a biologically detailed, stage-structured reaction-diffusion PDE model that tracks infected and uninfected mosquito populations across both aquatic and adult stages, while also incorporating spatial dispersion arising from mosquito flights. The PDE framework serves as a natural extension of previous ODE models [19, 38], retaining their biological structure while enabling the study of spatial thresholds, invasion waves, and heterogeneous environments within a mathematically tractable setting. Although our model employs isotropic diffusion for clarity and analytical simplicity, the framework can support future extensions such as spatially varying diffusion or nonlocal dispersal kernels to represent long-distance mosquito movement [23].

We systematically investigate how biological parameters influence the *Wolbachia* establishment threshold and spatial propagation using global sensitivity analysis. Additionally, we evaluate how release strategies—including pre-release mitigation, the choice of release location in regions with contrasting carrying capacities, and the timing of releases under seasonal environmental variation—affect the success and spatial spread of *Wolbachia* invasion. Our findings provide mechanistic insight into the nonlinear interplay between mosquito ecology, spatial structure, and intervention strategies, contributing to the design of efficient and sustainable *Wolbachia*-based vector-control programmes.

2 Methods

We developed a spatially explicit model that integrates the complex *Wolbachia* transmission dynamics with spatial heterogeneity and environmental variability. Building on our previous ODE framework [38], the current model incorporates spatial dispersion of adult mosquitoes via a reaction-diffusion approach, capturing the spread of infection and resulting travelling wave behaviour (Section 2.1). This spatial structure introduces challenges in characterising threshold conditions for *Wolbachia* invasion given a local mosquito release, which we explore in detail in Section 2.2.

To enhance biological realism, we refined model parametrisation of key life-history and transmission processes using laboratory and field data specific to the wMel strain of *Wolbachia* in *Aedes aegypti* mosquitoes (Section 2.3). Additionally, we introduced temporal heterogeneity by incorporating seasonal variation in temperature and rainfall, enabling the model to better reflect field conditions and assess the timing of intervention strategies.

2.1 Model formulation

The mosquito population is structured by life stages and infection status (Fig 1). We track uninfected and *Wolbachia*-infected cohorts separately, denoted by subscripts u and w, respectively. The model compartments include eggs (E_u and E_w), larvae/pupae combined (L_u and L_w), adult males (M_u and M_w), and adult females (F_u and F_w).

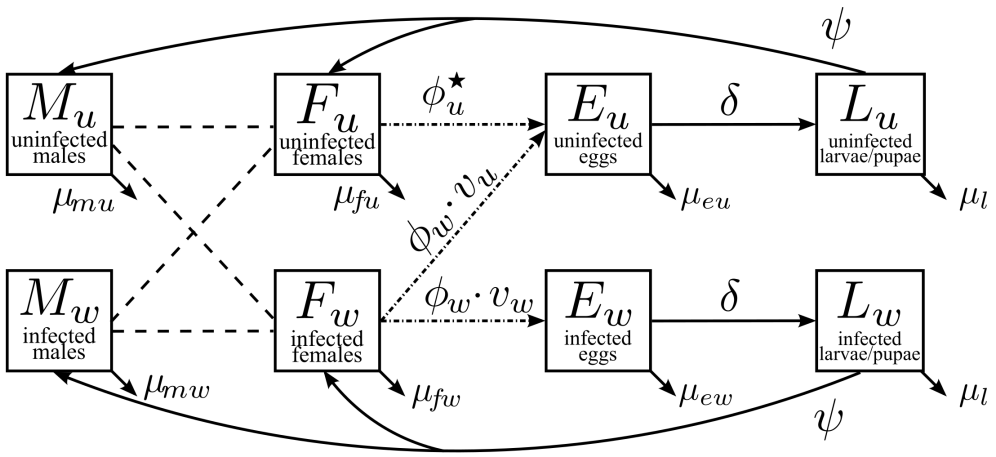

Fig 1: Flow diagram for the *Wolbachia*-maternal transmission throughout the mosquito life cycle, including the mating process between males and females (dashed lines), egg reproduction (dash-dotted arrows), and transitions between different life stages and mortality (solid arrows). Offspring production and viability depend on the infection status of both parents. Uninfected females (F_u) produce uninfected eggs at a rate $\phi_u^\star = \phi_u \frac{M_u}{M_u+M_w}$ when mating with uninfected males (M_u). No viable offspring result from the mating between F_u and infected males (M_w) due to cytoplasmic incompatibility. Infected females (F_w) lay eggs at a rate ϕ_w, with a fraction v_w being infected (E_w) and remaining $1 - v_w$ uninfected (E_u).

Wolbachia transmission follows a maternal inheritance pattern that depends on the infection status of the male and female mosquitoes at mating [4]. Infected females pass the infection to a fraction v_w of their offspring, resulting in infected eggs produced at a rate $v_w\phi_w$. Uninfected females, when mating with uninfected males, produce uninfected offspring at a rate of $\phi_u \frac{M_u}{M_u+M_w}$, where ϕ_u is the egg-laying rate for uninfected females. The term $\frac{M_u}{M_u+M_w}$ models the probability of encountering an uninfected male, assuming equal mating competence between the infected and uninfected males [39] and homogeneous mixing among males. When mating with infected males, the uninfected females produce non-viable offspring due to the *Wolbachia*-induced CI [2, 4].

Eggs hatch into larvae at a rate δ, and die at rates μ_{eu} and μ_{ew} for uninfected and infected cohorts, respectively. Larval and pupal stages (L_u, L_w) experience density-dependent regulation through a carrying

capacity K_l to account for resource competition at these stages. Larvae develop into adults at a rate ψ and die at a rate μ_l. Upon emergence, a fraction b_m becomes males and b_f becomes females. We assume that equal progression rates δ and ψ for infected and uninfected cohorts, as *Wolbachia* infection does not significantly affect these traits in *Aedes aegypti* mosquitoes [4]. The per-capita mortality rates for male mosquitoes are μ_{mu} and μ_{mw} for uninfected and infected individuals, respectively, and for females, they are μ_{fu} and μ_{fw}.

Adult mosquitoes engage in short-range, local dispersal through active flights. We model this movement using a diffusion process [40], which corresponds to a Gaussian distribution of flight distances, and assume that long-distance flights are rare. We include diffusion terms for all adult compartments, with diffusion coefficients $D_i (i = 1, \cdots, 4)$, representing the mean squared displacement per unit time. Juvenile-stage mosquitoes (eggs, larvae/pupae) remain confined to aquatic habitats until emergence; thus, no diffusion terms are assigned to these early life stages. This leads to a reaction-diffusion formulation, an approach widely used in spatial models of mosquito movements and *Wolbachia* spatial spread [34, 41] and is consistent with field studies showing that *Aedes aegypti* dispersal is predominantly local with limited long-range movement [42]. The estimated diffusion coefficients, described in Appendix B.2, were chosen to reproduce observed field-based dispersal ranges.

Based on these assumptions, the *Wolbachia* transmission dynamics are modelled using the following system of reaction-diffusion PDEs:

$$
\begin{aligned}
(E_u)_t &= \phi_u \frac{M_u}{M_u + M_w} F_u + (1 - v_w)\phi_w F_w - \delta E_u - \mu_{eu} E_u, \\
(E_w)_t &= v_w \phi_w F_w - \delta E_w - \mu_{ew} E_w, \\
(L_u)_t &= \delta E_u \left(1 - \frac{L_u + L_w}{K_l}\right) - \psi L_u - \mu_l L_u, \\
(L_w)_t &= \delta E_w \left(1 - \frac{L_u + L_w}{K_l}\right) - \psi L_w - \mu_l L_w, \\
(F_u)_t &= b_f \psi L_u - \mu_{fu} F_u + D_1 \Delta F_u, \\
(F_w)_t &= b_f \psi L_w - \mu_{fw} F_w + D_2 \Delta F_w, \\
(M_u)_t &= b_m \psi L_u - \mu_{mu} M_u + D_3 \Delta M_u, \\
(M_w)_t &= b_m \psi L_w - \mu_{mw} M_w + D_4 \Delta M_w.
\end{aligned}
$$

The state variables are defined as shown in Fig 1, and the model parameters and their baseline values are listed in Table 1. While the variable dependencies (on space x, y and time t) are suppressed in the system above for simplicity in presentation, both the mosquito life-history parameters (e.g., egg-laying rates, development rates, mortality) and carrying capacity can, in general, depend on environmental conditions, including temperature, rainfall, and habitat availability. In our later numerical simulations, we analyse both constant-parameter baselines and heterogeneous scenarios: (i) non-uniform and patchwise spatial heterogeneity in carrying capacity (Sections 3.2.3 and 3.3), and (ii) temperature- and rainfall-driven seasonal forcing of mosquito parameters and carrying capacity (Section 3.4). This allows us to assess the impact of environmental heterogeneity on the *Wolbachia* establishment and spatial propagation in a tractable manner.

Table 1: Model parameters and their baseline values for wMel strain of *Wolbachia* in *Aedes aegypti* mosquitoes. All rates are expressed in units of day^{-1}. We assume a perfect maternal transmission rate and complete cytoplasmic incompatibility [4, 10]. Parameters marked with † are *per capita* rates. Adjusted ranges are used for sensitivity analysis and are provided in Table C.3.

Parameters		Baseline	Range	Reference
b_f	Female birth probability	0.5		[4]
b_m	Male birth probability ($= 1 - b_f$)	0.5		[4]
ϕ_u	Egg-laying rate for uninfected females†	3.7	$1 \sim 8$	[10, 43, 44]
ϕ_w	Egg-laying rate for infected females†	3.5	$0.9 \sim 7.5$	[10, 43]
δ	Hatching rate for eggs†	1/2	$1/4 \sim 1$	[45, 46]
ψ	Development rate for larvae/pupae†	1/10	1/30∼1/8	[4, 46]
μ_{eu}	Mortality rate for uninfected eggs†	0.088	$0.08 \sim 0.17$	[10, 45]
μ_{ew}	Mortality rate for infected eggs†	0.185	$0.17 \sim 0.33$	[10, 45]
μ_l	Mortality rate for uninfected larvae/pupae†	0.12	$0.06 \sim 0.2$	[44]
μ_{fu}	Mortality rate for uninfected females†	1/17.5	$1/21 \sim 1/14$	[19, 47, 48]
μ_{fw}	Mortality rate for infected females†	1/15.8	$1/19 \sim 1/12.6$	[4]
μ_{mu}	Mortality rate for uninfected males†	1/10.5	$1/14 \sim 1/7$	[43]
μ_{mw}	Mortality rate for infected males†	1/10.5	$1/14 \sim 1/7$	[43]
v_w	Maternal transmission rate	1	$0.89 \sim 1$	[4, 10]
K_l	Carrying capacity of larvae stage (/m^2)	1		Assumed
D_i	Diffusion coefficients (m^2/day)	200	$100 \sim 300$	[23, 49, 50]

2.2 Threshold condition for *Wolbachia* invasion

2.2.1 Existence of a threshold

For *Wolbachia*-infected mosquitoes to successfully invade and replace the wild-type mosquitoes in the field, a threshold condition on the initial release is required. Previous ODE models have shown that this condition leads to bistable dynamics [19, 38]. Specifically, the system exhibits two distinct outcomes: if the infection level surpasses a critical threshold, *Wolbachia* infection can spread and stabilise at a high prevalence; otherwise, it dies out. Such bistability exists when the basic reproduction number for *Wolbachia* transmission among mosquitoes, $\mathcal{R}_0$, satisfies

$$4v_w(1 - v_w) \leq \mathcal{R}_0, \quad \mathcal{R}_0 = v_w \frac{\mu_{fu}\phi_w(\delta + \mu_{eu})}{\mu_{fw}\phi_u(\delta + \mu_{ew})}. \tag{1}$$

For baseline parametrisation, we have $v_w = 1$ (perfect maternal transmission), and condition Eq. (1) is automatically satisfied; the critical threshold infection frequency, characterised by the ODE model, is approximately 25%.

Our spatial PDE model retains these bistable dynamics while incorporating spatial complexity. In particular, adult mosquito dispersal introduces spatial heterogeneity in the threshold condition: the threshold level depends on the distance from the release centre, referred to as a "critical bubble" [20]. As illustrated in Fig 2, when the initial release (with compact support) is below a spatial threshold (panel A), the infection collapses. Conversely, when the infection exceeds the threshold, the infection establishes locally and propagates into nearby areas (panel B). The corresponding time series at the release centre (panel C) confirms the bistability in system dynamics.

2.2.2 Numerical identification of the threshold

To identify the spatial threshold or "critical bubble" for successful *Wolbachia* invasion, we adapt the numerical algorithm developed in [20], which leverages the bistable behaviour of the system. Specifically, we

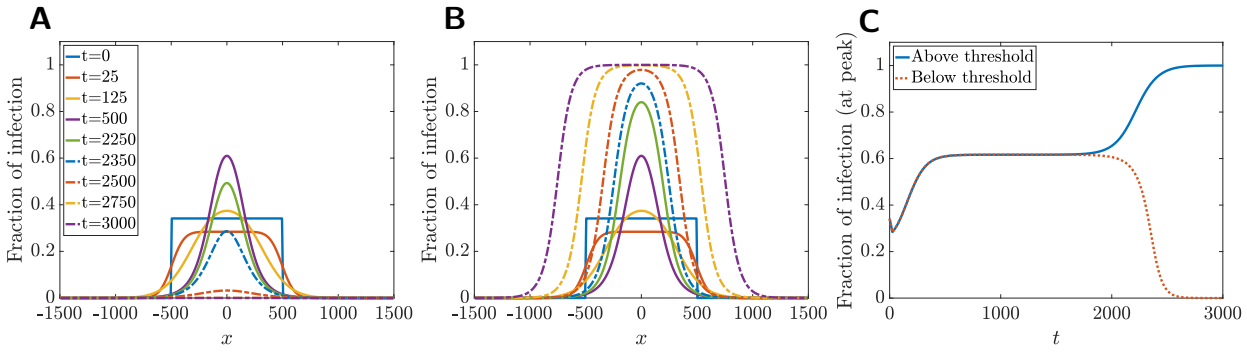

Fig 2: Threshold behaviour for *Wolbachia* establishment. (A) Fraction of infected females, $F_w/(F_u + F_w)$, under a step release with release radius $r = 500$ metres and release level $\approx 0.4169168378/m^2$. At $t = 0$, given $F_u \approx 0.80507567568/m^2$, this release level corresponds to an initial infection fraction ≈ 0.34117789857 at the release centre. The infection fails to persist, and the release is below the threshold. (B) Same numerical setting and legend as panel A, but with a slightly higher release level $\approx 0.4169168379/m^2$ (initial infection fraction ≈ 0.34117789864 at the release centre), for which the infection establishes locally and propagates outward when release exceeds the spatial threshold. In both panels A and B, the cross-sections of the solutions along the x-axis are shown, and the legend indicates the simulation time points at which the profiles are plotted. (C) Time series of the infection fraction at the release centre, $(x, y) = (0, 0)$, for simulations shown in panels A and B. After a brief transient phase, both trajectories approach an intermediate plateau for $500 \leq t \leq 1500$, corresponding to the formation of the critical bubble. The trajectories then diverge: the above-threshold release moves towards the high-infection stable state, while the below-threshold release collapses to the zero-infection state, illustrating the bistable dynamics of the system.

formulate a root-finding problem based on the time evolution of infection prevalence at the release centre:

$$\mathcal{J}(c) = 1 - 2 \times \underbrace{\left\{p_0(T;c) < p_0(T-\Delta t;c)\right\}}_{\text{Condition I}} - 2 \times \underbrace{\left\{|p_0(T;c)| < 10^{-4}\right\}}_{\text{Condition II}} + 2 \times \underbrace{\left\{|p_0(T;c) - p_{EE}| < 10^{-4}\right\}}_{\text{Condition III}} = 0, \tag{2}$$

where $p_0 = F_w/(F_u + F_w)$ denotes the fraction of infected females at the release centre $(x, y) = (0, 0)$, T is the final simulation time, Δt is the time step, and p_{EE} is the endemic equilibrium value of infection prevalence, analytically derived in [38, Eq. (9)].

The algorithm searches for a release level c^* (initial density of infected mosquitoes introduced per m^2), such that $\mathcal{J}(c^*) = 0$, providing an approximate threshold for invasion given a particular release shape. Each condition in Eq. (2) evaluates to 1 if true and 0 otherwise. For $c > c^*$, $p_0(t)$ approaches p_{EE} from below (blue solid curve in Fig 2C), resulting in $\mathcal{J}(c) > 0$ (Condition I = 0, II = 0, and III = 0 or 1 depending on T); For $c < c^*$, $p_0(t)$ approaches zero from above (red dotted curve in Fig 2C), leading to $\mathcal{J}(c) < 0$ (Condition I = 1, II = 0 or 1 depending T, and III = 0). Although an exact root may not exist, the algorithm yields a robust approximation of the transition point, which can be identified by the plateau in the time series near $t = 1000$ after which trajectories diverge towards their respective stable equilibria (Fig 2C).

Unless otherwise stated, our simulations use a step-shaped initial release with equal densities of infected males and females, $F_w(x, y, 0) = M_w(x, y, 0) = c$, over a disk $(x^2 + y^2 \leq r^2)$. We consider a range of release radii $50 \leq r \leq 500$ across numerical examples. Different values of r naturally lead to different threshold release level c^* for the step-function profile; however, all such initial conditions evolve towards the same critical bubble (with different transient dynamics though) [20]. This consistency is governed by the fact that the critical bubble is a non-trivial equilibrium of the PDE system. This algorithm is generalisable to other release distributions, such as the triangular distribution, and it yields comparable threshold profiles (Appendix A). We have used the step-shaped release throughout this study due to its field relevance.

2.3 Parametrisation and numerical method

All simulations were implemented in MATLAB 2024b, and the codes used to generate the figures and results are openly available in the associated GitHub repository [51]. Spatial derivatives were discretised using a fourth-order central difference scheme with free boundary conditions, and the time evolution was integrated using MATLAB `ODE45` solver.

Each simulation was initialised at *Wolbachia*-free equilibrium, modified by any pre-release mitigation strategy, and followed by the corresponding release scenario. Releases involved equal densities of infected males and females, referred to as the release level (in units of individuals per m^2), introduced uniformly within a disk-shaped region via a step function. The total release number is defined as the integral of the release level over the disk. Baseline parameter values for the wMel strain of *Wolbachia* in *Aedes aegypti* mosquitoes are listed in Table 1. Details of parameter derivation, including literature sources, are provided in Appendix B.

To assess the sensitivity of model outputs to parameter uncertainty, we perform a global sensitivity analysis (SA) using the Latin Hypercube Sampling/Pearson Partial Rank Correlation Coefficient (LHS/PRCC) technique. Five quantities of interest (QOIs) are evaluated, capturing characteristics of both the critical bubble (threshold level, total infection, and width) and the established infection wave (wave velocity and wave width). To ensure biological realism, fitness costs are imposed on *Wolbachia*-infected mosquitoes in the LHS parameter samples, including a reduced reproduction rate ($\phi_w < \phi_u$) and elevated mortality rates for infected females ($\mu_{fw} > \mu_{fu}$) and eggs ($\mu_{ew} > \mu_{eu}$), consistent with experimental findings [4, 10]. Full definitions of the QOIs and details of the sampling procedure are provided in Appendix C.

Both mosquito life-history traits and carrying capacity are sensitive to environmental conditions, particularly temperature and rainfall [46, 52]. To study how these variations may influence *Wolbachia* releases, we incorporate seasonality into the model (Section 3.4) using time-varying parameters, parametrised based on laboratory studies and empirical climate data. Further details are provided in Appendix B.3.

To assess the impact of spatial heterogeneity on the spatial spread of *Wolbachia* infection, we also incorporate patchwise carrying capacity (Section 3.3). In these simulations, the carrying capacity is defined as the piecewise function

$$K_l(x,y) = \begin{cases} K_l^{(1)}, & \text{if } x \le x^*, \\ K_l^{(2)}, & \text{if } x > x^*, \end{cases} \tag{3}$$

representing a transition between a lower-abundance "dry" region and a higher-abundance "wet" region. The left half of the domain is held at the baseline carrying capacity $K_l^{(1)}$, while the right half varies according to the specified carrying-capacity ratios. The wet-dry interface is set at the middle of the simulation domain, $x^* = 750$. This configuration provides a simplified but prototypical representation of spatial variation in habitat quality and allows us to examine how such heterogeneity generates asymmetric invasion dynamics.

3 Results

We conducted numerical simulations of the proposed spatial model to investigate *Wolbachia*-based intervention strategies, with a focus on scenarios relevant to field release programmes. The results aim to provide qualitative insights and inform the design of efficient and effective implementation strategies.

3.1 Critical bubbles and sensitivity analysis

We first examine the spatial threshold required for successful *Wolbachia* establishment at baseline parametrisation (Fig 3A). This threshold, referred to as the "critical bubble", exhibits a dome-shaped profile in the 2-D domain, with the highest infection rate required (approximately 60%) at the release centre $(x, y) = (0, 0)$ to support the initial local establishment of *Wolbachia*-infection and counteract the diffusion dynamics that may dilute the concentration of infection upon releases. The required infection level diminishes substantially with increasing distance from the centre, resulting in a steep infection gradient.

To assess the influence of spatial dimensionality and model complexity, we compare these results with those from 1-D simulations using the same diffusion parameters, and with a reduced two-PDE model that tracks only female mosquitoes [20]. In 1-D, the critical bubble generated by our full 8-PDE model is in close

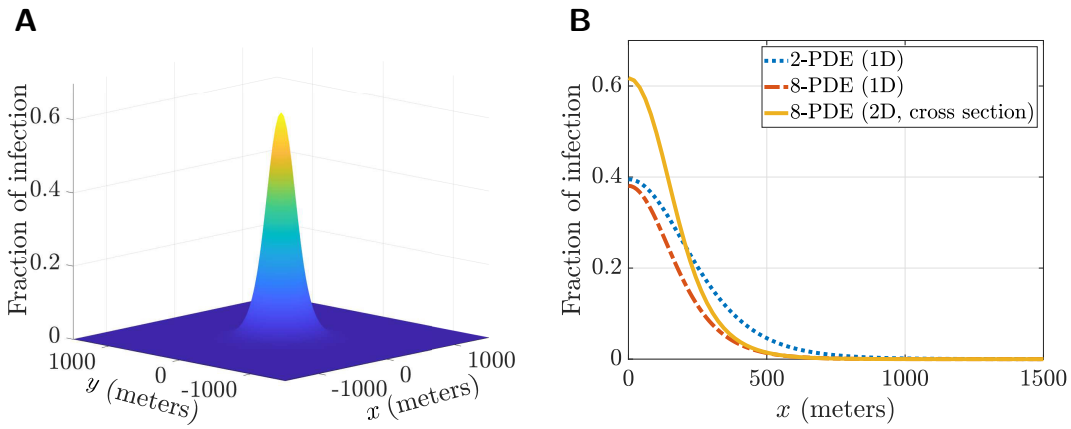

Fig 3: Threshold condition for sustainable *Wolbachia* releases. (A) The critical bubble, shown as the minimal spatial profile of infected female mosquitoes required for successful establishment, in a two-dimensional domain centred at $(x, y) = (0, 0)$. (B) Cross-sectional comparison of the critical bubble profile (from panel A) with corresponding profiles obtained from a reduced 2-PDE model [20] and from the full model in a one-dimensional domain. All subsequent simulations are conducted in 2D for biological realism.

agreement with its 2-PDE counterpart but is slightly lower and steeper (Fig 3B). This discrepancy likely arises from the inclusion of aquatic stages in our model, which have a zero-diffusion assumption and reduce the overall average diffusion in the system.

By contrast, the critical bubble in the 2-D is substantially higher, as the same diffusion coefficients represent a much greater amount of diffusion in 2-D compared to 1-D. While 2-D simulations incur greater computational cost, they offer improved biological realism for simulating field releases. We therefore focus on 2-D simulations in subsequent analyses.

We next assess the influence of model parameters on the critical bubble and the established *Wolbachia*-infection wave to identify key factors driving successful establishment and spread. The PRCC results (Fig 4 A–E) show that the maternal transmission rate (v_w; red) exhibits the strongest partial rank correlation across all QOIs considered, with PRCC exceeding 0.9 in absolute value for most quantities. Reproduction-related parameters (yellow), including egg survival (via μ_{eu}, μ_{ew} and δ) and female fitness traits (μ_{fu}, μ_{fw}, ϕ_u, and ϕ_w), show substantial influence on both the threshold level at the release centre (Fig 4B) and the spread of the infection wave (Fig 4D), with the PRCC in the range $0.3 \sim 0.8$. Diffusion coefficients (D_1, D_3; blue), along with male death rate (μ_{mu}), primarily affect the widths of both the critical bubble (Fig 4C) and the wave (Fig 4E), and also moderately affect wave velocity (Fig 4D). Notably, the female diffusion coefficient D_1 (with $D_2 = D_1$) has a dominating impact on wave width (Fig 4E), with a PRCC of 0.92, comparable in magnitude to that of v_w (PRCC $= -0.87$). In contrast, larval/pupal traits (μ_l, ψ; purple) are not significant for the threshold quantities (Figs. 4A–C), and exert only a modest but still statistically significant influence on wave velocity (Fig 4D).

3.2 Pre-release mitigation

Pre-release mitigation strategies, such as larviciding and spraying, aim to reduce the wild-type mosquito population prior to *Wolbachia* releases, thereby lowering the threshold required for a stable *Wolbachia* infection. To simulate this, we apply a fractional reduction θ to the targeted mosquito stages at the *Wolbachia*-free equilibrium. For example, an adult-stage intervention with efficacy θ reduces the uninfected female and male populations to $(1-\theta)F_u^0$ and $(1-\theta)M_u^0$, respectively.

We then examine how the threshold release number varies under different combinations of release radius (area where infected mosquitoes are introduced) and mitigation radius (area where uninfected mosquitoes are reduced), to identify optimal spatial coverage strategies for field implementation.

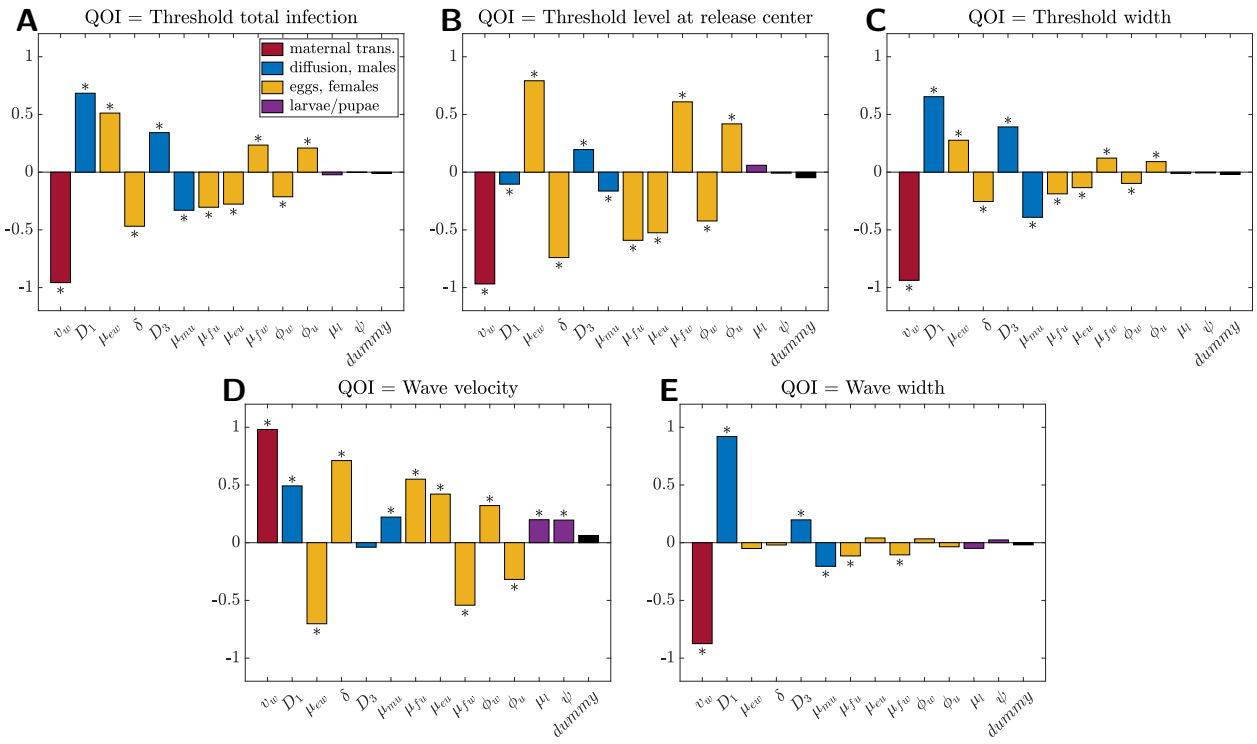

Fig 4: Global sensitivity analysis using PRCC for critical bubble characteristics and *Wolbachia*-infection wave properties. Panels show PRCC coefficients for different quantities of interest (QOI): (A) threshold total infection, (B) threshold level at the release centre, (C) threshold width, (D) wave velocity, and (E) wave width. The detailed definitions for the QOIs are specified in Appendix C.1. Bar colours correspond to parameter categories, as indicated in the legend in panel (A). A dummy parameter is included as a null comparison. Significance ($p < 0.05$) is marked with an asterisk (*).

3.2.1 Pre-release mitigation targeting adult mosquitoes

Pre-release mitigation targeting adults, such as space spraying or thermal fogging, can achieve reductions in adult mosquito densities of 50% $\sim$ 100% [53], though operational efficacy in diverse field conditions can be lower. With an efficacy of 80% ($\theta = 0.8$), it substantially reduces the threshold release number required for successful *Wolbachia* establishment by approximately 50% $\sim$ 60% over the range of release radii considered (Fig 5A). For a fixed mitigation radius, the threshold release number is consistently minimised when the release radius is around 200 metres (Fig 5B).

For a fixed release radius, increasing the pre-release mitigation radius reduces the threshold release number, following a sigmoidal trend (Fig 5C): reductions are slow at small mitigation radii, but there exists an inflection point, where the reduction is the fastest at a mitigation radius of around 100$\sim$150 metres. After this inflection point, the benefit of additional mitigation coverage diminishes, as the release number saturates. The inflection and the saturation points together inform the optimal pre-release mitigation coverage: ideally, the mitigation radius should at least reach the inflection point, to maximise efficiency per unit coverage, but extending far beyond the saturation point provides marginal benefit.

3.2.2 Pre-release mitigation targeting aquatic stages

We evaluate two pre-release mitigation strategies targeting aquatic stages: (1) drainage and scrubbing of water containers, which reduce juvenile stages (E_u^0 and L_u^0), and (2) larviciding, which impacts larvae/pupae stages (L_u^0) only. In both scenarios, breeding sites (i.e., water containers) remain available, so we assume the carrying capacity remains unchanged.

Both strategies show similar trends when varying the mitigation and release radii (Fig 5, panels D and E). Quantitatively, mitigation that targets all juvenile stages produces a threshold reduction up to approximately 6$\sim$24%, depending on the release radius. In contrast, targeting larvae/pupae alone yields a more modest 2$\sim$7% reduction (Fig 5F). Despite these improvements, aquatic-stage mitigation remains far less effective than adult-stage mitigation, which can reduce the threshold release number by up to 60% under comparable conditions (Fig 5C).

3.2.3 Pre-release mitigation via habitat modifications

Another common pre-release mitigation strategy involves habitat modifications that affect aquatic-stage mosquitoes by altering the availability of breeding sites. We considered two scenarios: (1) reducing breeding sites (e.g., removing water containers), which reduces all juvenile stages (E_u^0 and L_u^0) and the carrying capacity K_l; and (2) increasing breeding sites (adding containers with fresh water), which increases the carrying capacity K_l.

When breeding sites are reduced ($\theta = 0.3$), the threshold release number increases significantly (Fig 5G), by approximately 5% to 245% relative to the case without habitat modification (mitigation radius = 0), depending on the release radius. Notably, the threshold release number spikes when the mitigation radius approaches or slightly exceeds the release radius (dashed line in Fig 5G); the threshold release number drops again when the mitigation radius substantially exceeds the release radius (Fig 5I). This effect becomes more pronounced at higher reduction efficacy ($\theta = 0.5, 0.7$, Fig D.6 in appendix).

In contrast, increasing breeding sites ($\theta = -0.3$) can moderately lower the threshold release number, ranging from 3% to 42% depending on release radius. These reductions occur primarily when the release radius is small ($\leq$ 250 metres) and habitat modification is localised (mitigation radius $\leq$ 300 metres), see Fig 5, panels H and I. Overall, habitat modifications exert a weaker influence on threshold levels than adult-stage mitigation strategies.

3.3 Release infection in wet or dry regions

We examine the selection of release sites in regions with disparities in carrying capacities by comparing the releases in dry and wet regions.

When infection is released in the dry region (Fig 6A–C, dry-to-wet carrying capacity ratio 1 : 2.5), the infection wavefront slows substantially upon crossing into the wet region (around $t \approx 1500$) and enters the wet region only at $t \approx 4500$. This delay is caused by increased competition in the wet region, where the

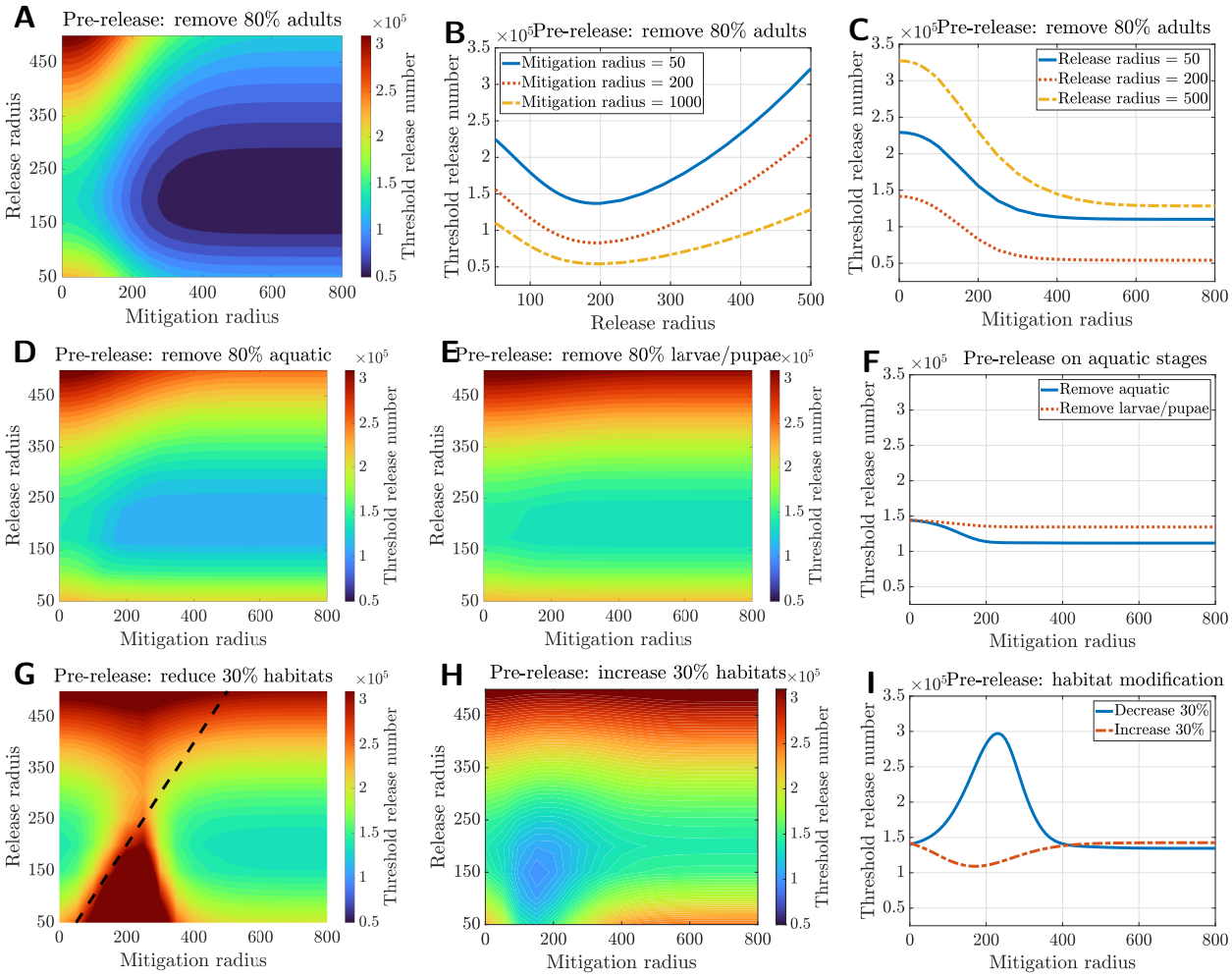

Fig 5: Impact of pre-release mitigation on threshold release number for *Wolbachia* establishment.
(A–C) Mitigation by removing 80% of adult mosquitoes (males and females): (A) Heatmap showing threshold release number as a function of mitigation radius and *Wolbachia* release radius. (B) Vertical slices of the heatmap (A) at fixed mitigation radii, indicating an optimal release radius of around 200 metres. (C) Horizontal slices of the heatmap (A) at fixed release radii, showing a sigmoidal decay in release numbers with increasing mitigation radius.
(D–F) Mitigation targeting aquatic stages: (D) Heatmap for removing 80% of aquatic-stage mosquitoes (eggs and larvae/pupae). (E) Heatmap for removing 80% of larvae/pupae only. (F) Horizontal slices of the heatmap (D) and (E) at a release radius of 200 metres, comparing their effects on threshold release number.
(G–I) Mitigation via habitat modifications: (G) Threshold release number when 30% of breeding sites are removed. The dashed line indicates where the mitigation radius equals the release radius. (H) Threshold release number when 30% of the breeding sites are added. (I) Horizontal slices of the heatmap in (G) and (H) at a release radius of 200 metres.

mosquito abundance is higher and proportional to the local carrying capacity. The delay is further illustrated in Fig 6F (solid curve), where the average fraction of infection across the domain shows a plateau between $t \approx 2500$ and $t \approx 4500$.

With stronger heterogeneity (e.g., carrying capacity ratio of 1 : 5), the wavefront may fail to propagate beyond the interface, as *Wolbachia*-infected mosquitoes are overwhelmed by the much denser wild-type population in the wet region (see Fig D.5, appendix). While increasing the initial release level accelerates the local establishment of the infection (Fig 6F, dotted curve), it does not improve wavefront propagation once the infection is established.

In contrast, releasing infection in the wet region allows the infection to propagate more easily into the dry region (Fig 6D and E). The infection wavefront even accelerates slightly when crossing the dry-wet interface (around $t \approx 1500$) due to the advantage of higher population abundance in the wet region (Fig 6F, dash-dotted curve). However, establishing *Wolbachia* from the wet region requires 2.5-fold the threshold release number needed for a release in the dry region, reflecting the increased threshold that scales with the higher carrying capacity.

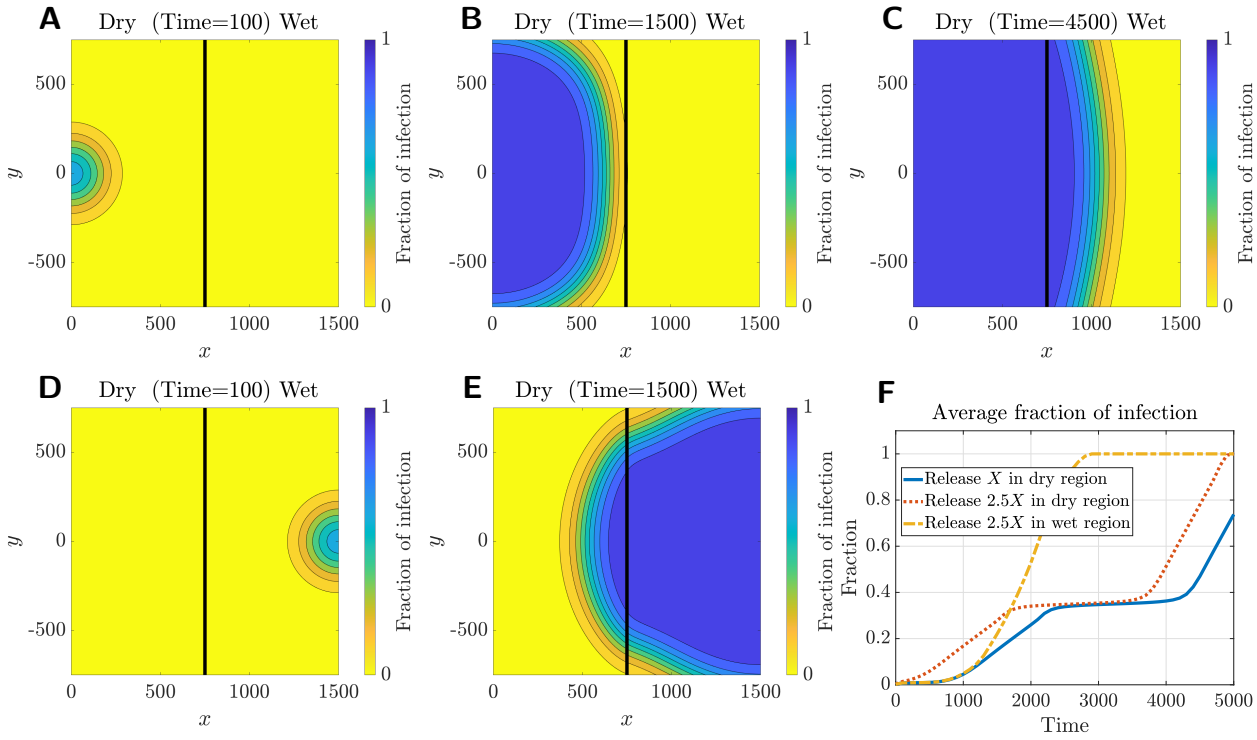

Fig 6: Simulations of *Wolbachia* establishment under heterogeneous habitat regions. The dry region ($x \leq 750$) has carrying capacity $1/m^2$, while the wet region ($x \geq 750$) has carrying capacity $2.5/m^2$.
(A–C): Release in the dry region at threshold level ($X \approx 5.8/m^2$ for both females and males), centred at (0,0) with release radius $r = 100$. The fraction of infected females is shown at $t = 100$ (A), $t = 1500$ (B), and $t = 4500$ (C), illustrating the temporal progression of the invasion.
(D–E): Release in the wet region at the corresponding threshold level ($2.5X \approx 14.6/m^2$), centred at (1500, 0) with $r = 100$. Panels show infection fraction at $t = 100$ (D) and $t = 1500$ (E).
(F): Time series of the average fraction of infection across the entire spatial domain for three release scenarios shown in the legend. (The spatial profile for wet-region $2.5X$ release is omitted in the figure, but its temporal average is included here in Panel F).

3.4 Impact of seasonality

The preceding simulations assumed constant model parameters, representing environments with minimal or no seasonal variation. Here, we focus on how seasonality affects the threshold for successful *Wolbachia* re-

leases, focusing on two real-world case studies: Yogyakarta, Indonesia, and Cairns, Australia, where *Wolbachia* programmes have been successfully implemented [9, 12]. These locations feature distinct climate profiles (Fig 7A and B), providing complementary scenarios to assess the timing and efficacy of releases.

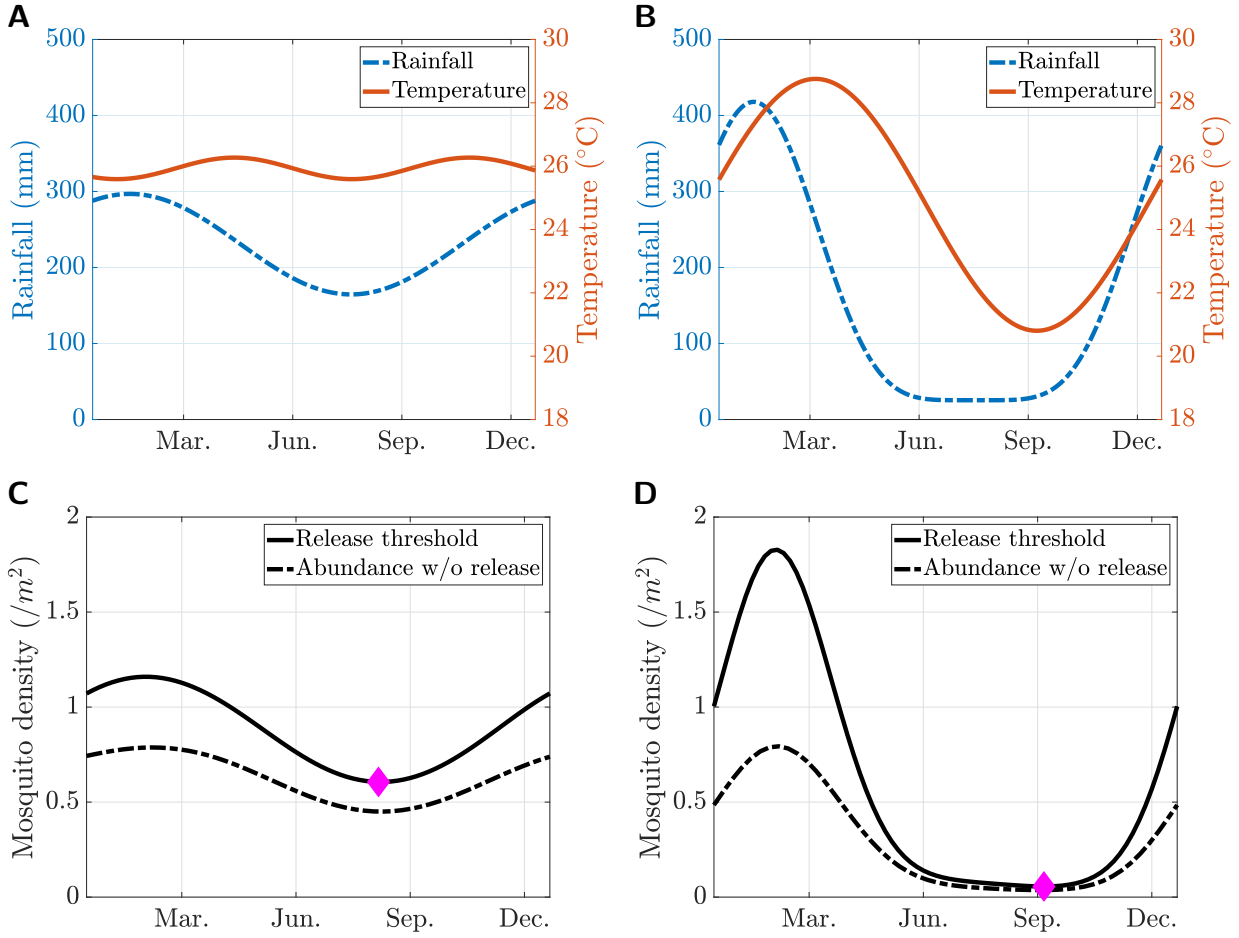

Fig 7: Impact of seasonality on *Wolbachia* population replacement thresholds. **(A–B)**: seasonal profiles for Yogyakarta, Indonesia (A) and Cairns, Australia (B), showing the rainfall (blue, left axis) and temperature (orange, right axis). **(C–D)**: Corresponding seasonal variation in the *Wolbachia* release threshold when deployed at different times (solid curve) and the natural abundance of uninfected mosquitoes in the absence of release (dashed curve), for Yogyakarta(C) and Cairns (D). The magenta diamond marks the minimal threshold release level within the annual cycle.

Yogyakarta has a tropical monsoon climate with moderate rainfall variation and minimal temperature changes, averaging around 26°C year-round (Fig 7A). Seasonal mosquito abundance (in the absence of *Wolbachia* releases) mirrors the rainfall patterns, with fewer mosquitoes during the dry season (Fig 7C, dashed curve). Simulations of different release timings (Fig 7C, solid curve) indicate that the optimal release window occurs around September (highlighted by the magenta diamond), when wild-type mosquito abundance is lowest, and competition from wild-type mosquitoes is minimised.

Cairns, in contrast, experiences stronger seasonal variations in both temperature and rainfall (Fig 7B), with a prolonged dry season from June to September. Correspondingly, mosquito abundance is highly seasonal (Fig 7D, dashed curve). Simulations show that the most effective time to release *Wolbachia*-infected mosquitoes is at the end of the dry season, just before the natural population begins to rise again (Fig 7D, solid curve). This timing minimises the competition from wild-type mosquitoes and takes advantage of the increasing mosquito abundance trend, which creates a favourable breeding condition for mosquitoes

in general and provides an opportunity for the *Wolbachia*-infected mosquitoes to efficiently outgrow the wild-type cohort.

4 Discussion

Our multistage spatial model integrates maternal transmission dynamics of *Wolbachia* across life stages with spatial dispersal of adults to evaluate the conditions required for successful *Wolbachia* establishment. Using the parametrisation for the wMel strain in *Aedes aegypti*, we numerically identify the critical spatial threshold – the "critical bubble" – needed for invasion in a 2-D domain. We further quantify how life-history traits, dispersal parameters, and environmental heterogeneity influence both the establishment threshold and wave propagation, and we assess how different pre-release mitigation strategies modify the release effort required for population replacement.

4.1 Insights from sensitivity analysis

Our sensitivity analysis highlights distinct mechanisms through which mosquito life-history traits influence the establishment and spatial spread of *Wolbachia* infection. Consistent with earlier modelling work [19, 38, 54], the maternal transmission rate emerges as the most impactful parameter across all threshold- and wave-related quantities. This reinforces the well-established role of maternal transmission as a key determinant of invasion potential in *Wolbachia* population replacement programmes [10].

Reproduction-related parameters, including egg survivorship, female fecundity, and female lifespan, also play an important role in determining the threshold level for invasion and subsequent velocity of the infection wave. Empirical studies report that *Wolbachia* infection can modulate fecundity and egg viability in strain-specific ways [55], and our results underscore the need for accurate estimation of these traits when assessing the field readiness of *Wolbachia* lines. In contrast, male life-history traits and diffusion coefficients primarily affect the geometry of the critical bubble and the spatial profile of the advancing wave rather than the overall feasibility of invasion [34]. Although males and their movements affect local mating structure, they only matter as the carriers of CI and play a secondary role in determining large-scale invasion outcomes.

Finally, the weak sensitivity of threshold quantities to larval and pupal traits reflects the assumption (also supported by laboratory observations [55]) that wMel imposes minimal fitness cost during early life stages as well as the impact of density dependence. As a result, the impact of variation in juvenile-stage parameters is offset by the density-dependent regulation, as strong larval competition buffers demographic fluctuations and contributes relatively little to competition between infected and uninfected cohorts [56].

4.2 Implications for pre-release mitigation strategies

Our results demonstrate clear differences in the effectiveness of pre-release mitigation strategies, depending on which mosquito life stages are targeted. Mitigation focused on adult mosquitoes consistently provides the greatest reduction in the release effort required for successful *Wolbachia* establishment. This aligns with the biological mechanism underlying *Wolbachia*-based population replacement, which is primarily driven by the reproductive advantage during the adult stages through cytoplasmic incompatibility [2, 4], reducing the overall fitness of the wild-type mosquitoes. Removing wild adult mosquitoes amplifies this mechanism by reducing competition for mates and breeding sites, which directly facilitates replacement.

In contrast, mitigation targeting aquatic stages—such as drainage or larval control—produces much smaller reductions in the release threshold. Notably, this diverges from the earlier non-spatial ODE model [38], which predicted comparable benefits in targeting adults and aquatic stages. The key distinction is that our spatial model incorporates adult mosquito diffusion, allowing *Wolbachia*-infected adults to rapidly disperse and occupy gaps created by pre-release reduction of adults upon release. This spatial spread amplifies the benefits of targeting adults—a feature absent from non-spatial frameworks.

Our findings also highlight that the benefits of adult-stage mitigation saturate beyond a certain spatial extent. Moreover, there is a consistent optimal release radius of approximately 200 metres under our parametrisation, regardless of the mitigation radius, assuming the same mitigation and release centres.

Mitigation strategies that modify habitat availability introduce additional complexity. From our simulations, reducing breeding sites before the release can increase the *Wolbachia* establishment threshold, and

the effect depends non-trivially on the spatial relationship between the mitigation and release radii. Two interacting mechanisms may underlie this behaviour. First, removing breeding sites reduces the local carrying capacity, intensifying density-dependent larval competition for both infected and uninfected cohorts and making it harder for the released infected cohort to breed and establish infection locally. Second, the sharp reduction in carrying capacity within the mitigation zone generates a steep spatial gradient in wild-type adult density at the mitigation boundary, driving an inward flux of uninfected adults from surrounding untreated areas. Both effects are most disruptive when the mitigation radius is close to the release radius, as the mitigation boundary then falls precisely at the edge of the release area, where local establishment is most critical for spatial invasion. As a result, for a fixed release radius, increasing the mitigation radius first elevates and then spikes the threshold as the mitigation radius approaches the release radius, before decreasing again once the mitigation radius extends sufficiently beyond the release zone and the wild-type gradient forms well outside the critical establishment region. These results are consistent with other modelling work, where limited breeding sites and the severity of density-dependent competition at the release sites can slow or greatly increase the release effort to establish *Wolbachia* [56, 57]. Our results also show that increasing breeding sites may modestly lower the threshold by providing an opportunity for *Wolbachia*-infected mosquitoes to establish dominance over the wild-type population, although the benefits are relatively small compared with adult-based pre-release interventions.

4.3 Effects of spatial and temporal heterogeneity

Spatial heterogeneity in habitat availability or carrying capacity can create strong asymmetries in how *Wolbachia* establishes and spreads across landscapes. In our simulations, releases initiated in low-abundance ("dry") regions require lower thresholds compared to those in high-abundance ("wet") regions. Once established, when the advancing infection wave encounters a dry-to-wet region transition, the infection wave propagation may slow or even stall, depending on the magnitude of the disparity. This is consistent with the empirical findings in [58], where neighbourhoods with higher baseline mosquito abundance can generate effective barriers for spatial spread and delay or impede the population replacement.

Seasonal climatic variability introduces another important source of environmental heterogeneity. By incorporating time-varying temperature and rainfall, our simulations indicate that the most favourable period for *Wolbachia* deployment is just before the onset of the wet season, when competition from natural mosquitoes is low, and the environment becomes more favourable for mosquito breeding, which creates an opportunity for the released mosquitoes to take over. This pattern aligns with other modelling studies showing that releasing in the early wet season requires smaller total release numbers to achieve establishment [59].

4.4 Model assumptions, limitations, and future directions

Our modelling results rely on several simplifying assumptions. First, we assumed equal and constant diffusion coefficients for female and male mosquitoes, consistent with field studies reporting no statistically significant difference in the mean distance travelled per day between sexes [42,49]. However, other studies report higher dispersal in males than females [60] or behavioural difference between gravid and unfed females [61]. Moreover, the reported dispersal varies widely in the literature and is strongly influenced by environmental factors, such as the spatial distribution of houses near the release site [60], wind patterns [62], and seasonal climatic conditions during collection [63]. These complexities introduce uncertainty in parametrising mosquito diffusion and highlight the need for models that incorporate sex-specific and environment-dependent movement behaviours.

Our model intentionally employs a standard diffusion formulation as a baseline spatial framework, corresponding to a Gaussian dispersal kernel and assuming that long-distance flights are rare. Our goal here is to evaluate how this simplified and widely used spatial representation shapes the threshold conditions for *Wolbachia* replacement, deferring more complex dispersal formulations to subsequent studies. Although this approximation is widely used, empirical data suggest that mosquito movement may exhibit non-Gaussian, fat-tailed patterns. Such kernels require an integro-differential or nonlocal PDE formulation, but can better capture the occasional long-range flights and landscape-driven heterogeneity, which may alter spatial dynamics. For example, fat-tailed kernels have been shown to substantially influence wave velocity and invasion patterns [23, 35]. Other work has incorporated switching between dispersal modes through slow–fast

or multiscale approaches to more accurately reflect observed flight behaviour [64]. Our modelling framework could be adapted to incorporate such nonlocal or hybrid dispersal mechanisms, which may enhance model realism and applicability in complex environmental settings.

Overall, our findings demonstrate that spatial structure, life-history traits, and environmental heterogeneity play critical roles in determining the conditions for successful *Wolbachia* replacement. By quantifying the spatial threshold and identifying how pre-release mitigation strategies and seasonal dynamics shape invasion potential, this work provides insight directly relevant to designing efficient field releases. Future extensions incorporating more realistic, field-informed habitat profiles and nonlocal dispersal mechanisms will further enhance the predictive power of spatial *Wolbachia* models and support the development of robust, context-specific vector-control programmes.

Acknowledgment

ZQ was partially supported by the National Science Foundation award DMS-2316242. The funder had no role in study design, data collection and analysis, decision to publish, or preparation of the manuscript.

References

1. Achee NL, Grieco JP, Vatandoost H, Seixas G, Pinto J, Ching-NG L, et al. Alternative Strategies for Mosquito-Borne Arbovirus Control. PLOS Neglected Tropical Diseases. 2019 Jan; doi: 10.1371/journal.pntd.000682213(1):e0006822.

2. Laven H. Eradication of Culex Pipiens Fatigans through Cytoplasmic Incompatibility. Nature. 1967; doi: 10.1038/216383a0216(5113):383-4.

3. McMeniman CJ, Lane RV, Cass BN, Fong AWC, Sidhu M, Wang YF, et al. Stable Introduction of a Life-Shortening Wolbachia Infection into the Mosquito Aedes Aegypti. Science. 2009; doi: 10.1126/science.1165326323(5910):141-4.

4. Walker T, Johnson PH, Moreira LA, Iturbe-Ormaetxe I, Frentiu FD, McMeniman CJ, et al. The wMel Wolbachia Strain Blocks Dengue and Invades Caged Aedes Aegypti Populations. Nature. 2011 Aug; doi: 10.1038/nature10355476(7361):450-3.

5. Alphey L, Benedict M, Bellini R, Clark GG, Dame DA, Service MW, et al. Sterile-Insect Methods for Control of Mosquito-Borne Diseases: An Analysis. Vector Borne Zoonotic Dis. 2010; doi: 10.1089/vbz.2009.001410(3):295-311.

6. Lofgren CS, Dame DA, Breeland SG, Weidhaas DE, Jeffery G, Kaiser R, et al. Release of Chemosterilized Males for the Control of Anopheles Albimanus in El Salvador: III. Field Methods and Population Control. The American Journal of Tropical Medicine and Hygiene. 1974 Mar; doi: 10.4269/ajtmh.1974.23.28823(2):288-97.

7. Alphey L. Genetic Control of Mosquitoes. Annual Review of Entomology. 2014 Jan; doi: 10.1146/annurev-ento-011613-16200259(1):205-24.

8. Kyrou K, Hammond AM, Galizi R, Kranjc N, Burt A, Beaghton AK, et al. A CRISPR–Cas9 Gene Drive Targeting Doublesex Causes Complete Population Suppression in Caged Anopheles Gambiae Mosquitoes. Nature Biotechnology. 2018 Nov; doi: 10.1038/nbt.424536(11):1062-6.

9. Hoffmann AA, Montgomery BL, Popovici J, Iturbe-Ormaetxe I, Johnson PH, Muzzi F, et al. Successful Establishment of Wolbachia in Aedes Populations to Suppress Dengue Transmission. Nature. 2011 Aug; doi: 10.1038/nature10356476(7361):454-7.

10. Hoffmann AA, Iturbe-Ormaetxe I, Callahan AG, Phillips BL, Billington K, Axford JK, et al. Stability of the wMel Wolbachia Infection Following Invasion into Aedes Aegypti Populations. PLoS Negl Trop Dis. 2014; doi: 10.1371/journal.pntd.00031158(9):e3115.

11. Ryan PA, Turley AP, Wilson G, Hurst TP, Retzki K, Brown-Kenyon J, et al. Establishment of wMel Wolbachia in Aedes Aegypti Mosquitoes and Reduction of Local Dengue Transmission in Cairns and Surrounding Locations in Northern Queensland, Australia [Version 2; Peer Review: 2 Approved]. Gates Open Research. 2020; doi: 10.12688/gatesopenres.13061.23(1547).

12. Indriani C, Tantowijoyo W, Rancès E, Andari B, Prabowo E, Yusdi D, et al. Reduced Dengue Incidence Following Deployments of Wolbachia-infected Aedes Aegypti in Yogyakarta, Indonesia: A Quasi-Experimental Trial Using Controlled Interrupted Time Series Analysis. Gates Open Research. 2020 May; doi: 10.12688/gatesopenres.13122.14:50.

13. Bian G, Joshi D, Dong Y, Lu P, Zhou G, Pan X, et al. Wolbachia Invades Anopheles Stephensi Populations and Induces Refractoriness to Plasmodium Infection. Science. 2013 May; doi: 10.1126/science.1236192340(6133):748-51.

14. Joshi D, McFadden MJ, Bevins D, Zhang F, Xi Z. Wolbachia Strain w AlbB Confers Both Fitness Costs and Benefit on Anopheles Stephensi. Parasites & Vectors. 2014 Dec; doi: 10.1186/1756-3305-7-3367(1):336.

15. Gomes FM, Barillas-Mury C. Infection of Anopheline Mosquitoes with Wolbachia: Implications for Malaria Control. PLOS Pathogens. 2018 Nov; doi: 10.1371/journal.ppat.100733314(11):e1007333.

16. Axford JK, Ross PA, Yeap HL, Callahan AG, Hoffmann AA. Fitness of wAlbB Wolbachia Infection in Aedes Aegypti: Parameter Estimates in an Outcrossed Background and Potential for Population Invasion. The American Journal of Tropical Medicine and Hygiene. 2016 Mar; doi: 10.4269/ajtmh.15-060894(3):507-16.

17. Jiggins FM. The Spread of Wolbachia through Mosquito Populations. PLOS Biology. 2017 Jun; doi: 10.1371/journal.pbio.200278015(6):e2002780.

18. Koiller J, Da Silva M, Souza M, Codeço C, Iggidr A, Sallet G. Aedes, Wolbachia and Dengue. Inria Nancy-Grand Est, Villers-lès-Nancy, France; 2014. RR-8462.

19. Qu Z, Xue L, Hyman JM. Modeling the Transmission of Wolbachia in Mosquitoes for Controlling Mosquito-Borne Diseases. SIAM Journal on Applied Mathematics. 2018 Jan; doi: 10.1137/17M113080078(2):826-52.

20. Qu Z, Wu T, Hyman JM. Modeling Spatial Waves of Wolbachia Invasion for Controlling Mosquito-Borne Diseases. SIAM Journal on Applied Mathematics. 2022.

21. Xue L, Manore CA, Thongsripong P, Hyman JM. Two-Sex Mosquito Model for the Persistence of Wolbachia. Journal of Biological Dynamics. 2016; doi: 10.1080/17513758.2016.122905111(sup1):216-37.

22. Ndii MZ, Wiraningsih ED, Anggriani N, Supriatna AK. Mathematical Model as a Tool for the Control of Vector-Borne Diseases: Wolbachia Example. In: Falcón-Lezama JA, Betancourt-Cravioto M, Tapia-Conyer R, editors. Dengue Fever-A Resilient Threat in the Face of Innovation. London: IntechOpen; 2018. .

23. Turelli M, Barton NH. Deploying Dengue-Suppressing Wolbachia : Robust Models Predict Slow but Effective Spatial Spread in Aedes Aegypti. Theoretical Population Biology. 2017 Jun; doi: 10.1016/j.tpb.2017.03.003115:45-60.

24. Ferguson NM, Hue Kien DT, Clapham H, Aguas R, Trung VT, Bich Chau TN, et al. Modeling the Impact on Virus Transmission of Wolbachia-mediated Blocking of Dengue Virus Infection of Aedes Aegypti. Science Translational Medicine. 2015 Mar; doi: 10.1126/scitranslmed.30103707(279).

25. Childs LM, Hughes R, Blackwood JC. The Role of Increased Gonotrophic Cycles in the Establishment of Wolbachia in Anopheles Populations. Theoretical Ecology. 2020 Sep; doi: 10.1007/s12080-020-00457-813(3):349-69.

26. Zhang X, Tang S, Cheke RA. Models to Assess How Best to Replace Dengue Virus Vectors with Wolbachia -Infected Mosquito Populations. Mathematical Biosciences. 2015 Nov; doi: 10.1016/j.mbs.2015.09.004269:164-77.

27. Dye D, Cain JW. Efficacy of Wolbachia-based Mosquito Control: Predictions of a Spatially Discrete Mathematical Model. PLOS ONE. 2024 Mar; doi: 10.1371/journal.pone.029796419(3):e0297964.

28. Hancock PA, Ritchie SA, Koenraadt CJM, Scott TW, Hoffmann AA, Godfray HCJ. Predicting the Spatial Dynamics of *Wolbachia* Infections in *Aedes Aegypti* Arbovirus Vector Populations in Heterogeneous Landscapes. Journal of Applied Ecology. 2019 Jul; doi: 10.1111/1365-2664.1342356(7):1674-86.

29. Barlow A, Adams B. Household Scale Wolbachia Release Strategies for Effective Dengue Control. Ecological Modelling. 2026 Jan; doi: 10.1016/j.ecolmodel.2025.111384511:111384.

30. Eckhoff PA, Wenger EA, Godfray HCJ, Burt A. Impact of Mosquito Gene Drive on Malaria Elimination in a Computational Model with Explicit Spatial and Temporal Dynamics. Proceedings of the National Academy of Sciences. 2017 Jan; doi: 10.1073/pnas.1611064114114(2).

31. Magori K, Legros M, Puente ME, Focks DA, Scott TW, Lloyd AL, et al. Skeeter Buster: A Stochastic, Spatially Explicit Modeling Tool for Studying Aedes Aegypti Population Replacement and Population Suppression Strategies. PLoS Neglected Tropical Diseases. 2009 Sep; doi: 10.1371/journal.pntd.00005083(9):e508.

32. Mondal A, Sánchez C HM, Marshall JM. MGDrivE 3: A Decoupled Vector-Human Framework for Epidemiological Simulation of Mosquito Genetic Control Tools and Their Surveillance. PLOS Computational Biology. 2024 May; doi: 10.1371/journal.pcbi.101213320(5):e1012133.

33. North A, Burt A, Godfray HCJ. Modelling the Spatial Spread of a Homing Endonuclease Gene in a Mosquito Population. Journal of Applied Ecology. 2013 Oct; doi: 10.1111/1365-2664.1213350(5):1216-25.

34. Barton NH, Turelli M. Spatial Waves of Advance with Bistable Dynamics: Cytoplasmic and Genetic Analogues of Allee Effects. The American Naturalist. 2011 Sep; doi: 10.1086/661246178(3):E48-75.

35. Schofield P. Spatially Explicit Models of Turelli-Hoffmann Wolbachia Invasive Wave Fronts. Journal of Theoretical Biology. 2002; doi: 10.1006/jtbi.2001.2493215(1):121-31.

36. Huang M, Tang M, Yu J. Wolbachia Infection Dynamics by Reaction-Diffusion Equations. Science China Mathematics. 2015 Jan; doi: 10.1007/s11425-014-4934-858(1):77-96.

37. Duprez M, Hélie R, Privat Y, Vauchelet N. Optimization of Spatial Control Strategies for Population Replacement, Application to *Wolbachia*. ESAIM: Control, Optimisation and Calculus of Variations. 2021; doi: 10.1051/cocv/202107027:74.

38. Florez D, Young AJ, Bernabé KJ, Hyman JM, Qu Z. Modeling Sustained Transmission of Wolbachia among Anopheles Mosquitoes: Implications for Malaria Control in Haiti. Tropical Medicine and Infectious Disease. 2023 Mar; doi: 10.3390/tropicalmed80301628(3):162.

39. Segoli M, Hoffmann AA, Lloyd J, Omodei GJ, Ritchie SA. The Effect of Virus-Blocking Wolbachia on Male Competitiveness of the Dengue Vector Mosquito, Aedes Aegypti. PLoS Negl Trop Dis. 2014; doi: 10.1371/journal.pntd.00032948(12):e3294.

40. Takahashi L, Maidana N, Ferreirajr W, Pulino P, Yang H. Mathematical Models for the Dispersal Dynamics: Travelling Waves by Wing and Wind. Bulletin of Mathematical Biology. 2005 May; doi: 10.1016/j.bulm.2004.08.00567(3):509-28.

41. Hughes H, Britton NF. Modelling the Use of Wolbachia to Control Dengue Fever Transmission. Bulletin of Mathematical Biology. 2013; doi: 10.1007/s11538-013-9835-475(5):796-818.

42. HARRINGTON LC, SCOTT TW, LERDTHUSNEE K, COLEMAN RC, COSTERO A, CLARK GG, et al. Dispersal of the Dengue Vector Aedes Aegypti within and between Rural Communities. The American Journal of Tropical Medicine and Hygiene,. 2005; doi: 10.4269/ajtmh.2005.72.20972(2):209-20.

43. Styer LM, Minnick SL, Sun AK, Scott TW. Mortality and Reproductive Dynamics of Aedes Aegypti (Diptera: Culicidae) Fed Human Blood. Vector Borne Zoonotic Dis. 2007; doi: 10.1089/vbz.2007.02167(1):86-98.

44. Yang HM, Macoris MdLdG, Galvani KC, Andrighetti MTM. Follow up Estimation of Aedes Aegypti Entomological Parameters and Mathematical Modellings. Biosystems. 2011 Mar; doi: 10.1016/j.biosystems.2010.11.002103(3):360-71.

45. Soares-Pinheiro VC, Dasso-Pinheiro W, Trindade-Bezerra JM, Tadei WP. Eggs Viability of Aedes Aegypti Linnaeus (Diptera, Culicidae) under Different Environmental and Storage Conditions in Manaus, Amazonas, Brazil. Brazilian Journal of Biology. 2016 Aug; doi: 10.1590/1519-6984.1981577(2):396-401.

46. Foster WA, Walker ED. Mosquitoes (Culicidae). In: Medical and Veterinary Entomology. Amsterdam: Academic Press; 2002. p. 203-62.

47. Zettel C, Kaufman P. Yellow Fever Mosquito Aedes Aegypti (Linnaeus) (Insecta: Diptera: Culicidae): EENY-434/IN792, 2/2009. EDIS. 2009 Apr; doi: 10.32473/edis-in792-20092009(2).

48. National Environment Agency. Aedes Mosquito; 2020. https://www.nea.gov.sg/dengue-zika/prevent-aedes-mosquito-breeding/aedes-mosquito.

49. Kay BH, Muir LE. Aedes Aegypti Survival and Dispersal Estimated by Mark-Release-Recapture in Northern Australia. The American Journal of Tropical Medicine and Hygiene. 1998 Mar; doi: 10.4269/ajtmh.1998.58.27758(3):277-82.

50. Russell RC, Webb CE, Williams CR, Ritchie SA. Mark-Release-Recapture Study to Measure Dispersal of the Mosquito Aedes Aegypti in Cairns, Queensland, Australia. Medical and Veterinary Entomology. 2005 Dec; doi: 10.1111/j.1365-2915.2005.00589.x19(4):451-7.

51. Qu Z, Wu T. Multistage spatial model for informing release of Wolbachia-infected mosquitoes as disease control. GitHub; 2025. Available from: https://github.com/zhuolinqu/Wolbachia-Spatial.

52. Reinhold J, Lazzari C, Lahondère C. Effects of the Environmental Temperature on Aedes Aegypti and Aedes Albopictus Mosquitoes: A Review. Insects. 2018 Nov; doi: 10.3390/insects90401589(4):158.

53. Pryce J, Choi L, Richardson M, Malone D. Insecticide Space Spraying for Preventing Malaria Transmission. Cochrane Database of Systematic Reviews. doi: 10.1002/14651858.CD012689.pub22018 Nov.

54. Zheng B, Tang M, Yu J, Qiu J. Wolbachia Spreading Dynamics in Mosquitoes with Imperfect Maternal Transmission. Journal of Mathematical Biology. 2018 Jan; doi: 10.1007/s00285-017-1142-576(1-2):235-63.

55. Allman MJ, Fraser JE, Ritchie SA, Joubert DA, Simmons CP, Flores HA. Wolbachia's Deleterious Impact on Aedes Aegypti Egg Development: The Potential Role of Nutritional Parasitism. Insects. 2020 Oct; doi: 10.3390/insects1111073511(11):735.

56. Hancock PA, White VL, Callahan AG, Godfray CHJ, Hoffmann AA, Ritchie SA. Density-Dependent Population Dynamics in *Aedes Aegypti* Slow the Spread of *w* Mel *Wolbachia*. Journal of Applied Ecology. 2016 Jun; doi: 10.1111/1365-2664.1262053(3):785-93.

57. Hancock PA, White VL, Ritchie SA, Hoffmann AA, Godfray HCJ. Predicting Wolbachia Invasion Dynamics in Aedes Aegypti Populations Using Models of Density-Dependent Demographic Traits. BMC Biology. 2016 Nov; doi: 10.1186/s12915-016-0319-514:96.

58. Schmidt TL, Barton NH, Rašić G, Turley AP, Montgomery BL, Iturbe-Ormaetxe I, et al. Local Introduction and Heterogeneous Spatial Spread of Dengue-Suppressing Wolbachia through an Urban Population of Aedes Aegypti. PLOS Biology. 2017 May; doi: 10.1371/journal.pbio.200189415(5):e2001894.

59. Hancock PA, Sinkins SP, Godfray HCJ. Strategies for Introducing Wolbachia to Reduce Transmission of Mosquito-Borne Diseases. PLoS neglected tropical diseases. 2011 Apr; doi: 10.1371/journal.pntd.00010245(4):e1024.

60. Tsuda Y, Takagi M, Wang S, Wang Z, Tang L. Movement of Aedes Aegypti (Diptera: Culicidae) Released in a Small Isolated Village on Hainan Island, China. Journal of Medical Entomology. 2001 Jan; doi: 10.1603/0022-2585-38.1.9338(1):93-8.

61. Juarez JG, Garcia-Luna S, Chaves LF, Carbajal E, Valdez E, Avila C, et al. Dispersal of Female and Male Aedes Aegypti from Discarded Container Habitats Using a Stable Isotope Mark-Capture Study Design in South Texas. Scientific Reports. 2020 Apr; doi: 10.1038/s41598-020-63670-910(1):6803.

62. Garrett-Jones C. A Dispersion of Mosquitoes by Wind. Nature. 1950; doi: 10.1038/165285a0165(4190):285-5.

63. Mains JW, Kelly PH, Dobson KL, Petrie WD, Dobson SL. Localized Control of Aedes Aegypti (Diptera: Culicidae) in Miami, FL, via Inundative Releases of Wolbachia-Infected Male Mosquitoes. Journal of Medical Entomology. 2019 Sep; doi: 10.1093/jme/tjz05156(5):1296-303.

64. Chan MHT, Kim PS. Modelling a Wolbachia Invasion Using a Slow-Fast Dispersal Reaction-Diffusion Approach. Bulletin of Mathematical Biology. 2013 Sep; doi: 10.1007/s11538-013-9857-y75(9):1501-23.

65. Silva MR, Lugão PHG, Chapiro G. Modeling and Simulation of the Spatial Population Dynamics of the Aedes Aegypti Mosquito with an Insecticide Application. Parasites & Vectors. 2020 Dec; doi: 10.1186/s13071-020-04426-213(1):550.

66. Morris CD, Larson VL, Lounibos LP. Measuring Mosquito Dispersal for Control Programs. Journal of the American Mosquito Control Association. 1991 Dec;7(4):608-15.

67. National Oceanic and Atmospheric Administration (NOAA). NOAA Climate Data Online. NOAA;. https://www.ncei.noaa.gov/cdo-web/.

68. World Bank Group. Climate Change Knowledge Portal; 2021. https://climateknowledgeportal.worldbank.org/.

69. Mordecai EA, Cohen JM, Evans MV, Gudapati P, Johnson LR, Lippi CA, et al. Detecting the Impact of Temperature on Transmission of Zika, Dengue, and Chikungunya Using Mechanistic Models. PLOS Neglected Tropical Diseases. 2017 Apr; doi: 10.1371/journal.pntd.000556811(4):e0005568.

70. Farnesi LC, Martins AJ, Valle D, Rezende GL. Embryonic Development of Aedes Aegypti (Diptera: Culicidae): Influence of Different Constant Temperatures. Memórias do Instituto Oswaldo Cruz. 2009 Feb; doi: 10.1590/S0074-027620090000100020104(1):124-6.

71. Valdez LD, Sibona GJ, Condat CA. Impact of Rainfall on Aedes Aegypti Populations. Ecological Modelling. 2018 Oct; doi: 10.1016/j.ecolmodel.2018.07.003385:96-105.

72. Tran A, L'Ambert G, Lacour G, Benoît R, Demarchi M, Cros M, et al. A Rainfall- and Temperature-Driven Abundance Model for Aedes Albopictus Populations. International Journal of Environmental Research and Public Health. 2013 Apr; doi: 10.3390/ijerph1005169810(5):1698-719.

Supplementary material to: Multistage spatial model for informing release of *Wolbachia*-infected mosquitoes as disease control

Zhuolin Qu[1*], Tong Wu[1]

1 Department of Mathematics, University of Texas at San Antonio, San Antonio, TX, United States of America

* Corresponding author
Email: zhuolin.qu@utsa.edu

A Critical bubble under different release shapes

The threshold identification algorithm described in Section 2.2.2 can be applied to a range of initial release distributions. Despite differences in spatial configuration, the resulting critical bubble is robust to the shape of the initial release.

Fig A.1 compares the threshold profiles obtained using step-shaped, triangular, and elliptical distributions. In each case, when the release intensity is tuned to its respective threshold level, the infection evolves towards similar spatial threshold structures, demonstrating the consistency of the critical bubble across different initial conditions.

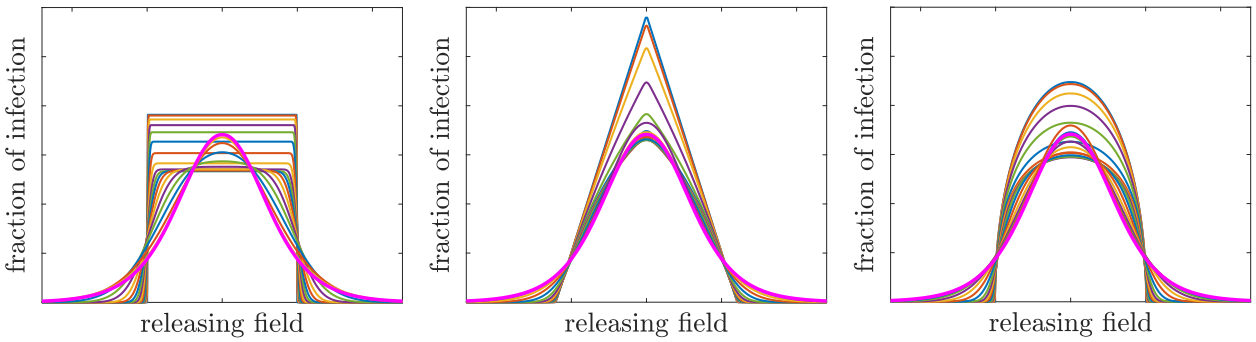

Fig A.1: Robustness of the critical bubble under different initial release shapes: step-shaped (left), triangular (centre), and elliptical (right) distributions converge to the same threshold profile (magenta curves).

B Detailed parametrisation and methods

B.1 Mosquito-related parameters

Baseline parameter estimates and ranges are provided in Table 1 in the main text. Parametrisation draws upon biological studies of *Aedes aegypti* life-history traits, the effects of *Wolbachia* infection, and data from recent field releases, particularly those conducted in Australia. Recognising that certain parameters are highly influenced by local environmental conditions, we incorporated data from both laboratory experiments and field trials for more informed and context-specific estimates.

Adult lifespan In laboratory settings, the lifespan of female *Aedes aegypti* mosquitoes can reach up to 70 days [4, Figure S6]. However, for field conditions, we adopted a more conservative estimate of approximately two weeks (17.5 days) [47, 48]. We assumed that the male lifespan is about 1.5 weeks, roughly 60% of the female lifespan [4, 43].

For *Wolbachia*-infected adults, a reduction in longevity of approximately 10% has been reported for infected females [4, Supplementary Figure S6]. Accordingly, we set the infected female lifespan to $1/\mu_{fw} = 0.9/\mu_{fu}$, while assuming no difference in male longevity, i.e., $\mu_{mu} = \mu_{mw}$.

Fecundity In laboratory cage experiments, no significant differences in mean fecundity were observed between infected and uninfected cohorts, with both producing approximately 105 eggs per female [4, Figure S4]. However, from the field release estimates [10], there is a reduction in the number of eggs laid by *Wolbachia*-infected females compared to uninfected females, with uninfected females producing approximately 65 eggs per female and infected females producing 55 eggs per female.

Using these field estimates and dividing by the corresponding female lifespans, we estimate egg-laying rates of approximately 3.7 eggs/day for uninfected females (65/17.5) and 3.5 eggs/day for the infected females (55/15.8). These values are consistent with ranges observed in laboratory experiments [43].

Eggs Egg death rates and hatching rates (number of eggs hatched per unit time) are not directly reported in the biological literature. Instead, we rely on estimates of egg viability (the fraction of eggs that become larvae, $\delta/(\delta+\mu_E)$, and the egg hatching period $(1/\delta)$.

In laboratory studies, wMel-infected females mated to both uninfected and wMel-infected males showed embryo hatch rates of approximately 90% [4, Table S1], with no significant differences observed between the mean hatch rates of infected and uninfected lines [4, Figure S5]. However, in field releases, egg hatching rates were reported as 85% for uninfected eggs (range: 75% $\sim$ 86%) and 73% for infected eggs (range: 60% $\sim$ 75%) [10], suggesting that $\mu_{eu} \neq \mu_{ew}$. Using these values, we establish the following relations:

$$\frac{\delta_u}{\delta_u+\mu_{eu}} = 0.85, \quad \frac{\delta_w}{\delta_w+\mu_{ew}} = 0.73.$$

The egg hatching period is approximately 2 days [45], with a range of $1 \sim 4$ days, depending on temperature [46]. Thus, we assume $\delta_u = \delta_w = \delta = 1/2$, and using the relation above, we estimate egg death rates as $\mu_{eu} = 0.088$ (range: $0.08 \sim 0.17$), and $\mu_{ew} = 0.185$ (range: $0.17 \sim 0.33$).

Overall, the total number of viable eggs produced is approximately 55.25 eggs/female for uninfected mosquitoes (65 eggs/female $\times$85%) and 40.15 eggs/female for infected mosquitoes (55 eggs/female $\times$73%). This represents a fitness cost in infected female fecundity of about 27%, consistent with estimates in the literature (24%, [4, 10]).

Larvae The mortality rate during the larvae/pupae stage was estimated as $\mu_l \sim 0.12$/day in [44]. The wMel infection does not appear to affect the development time [4], so we assume the development time from larvae to adults is approximately 10 days under field conditions [44], with a broad range of $8 \sim 30$ days, depending on food availability and temperature [4, 46, Table S2].

***Wolbachia* transmission** We assumed a complete cytoplasmic incompatibility (CI) effect [4, 10, Table S1] and perfect maternal transmission, $v_w = 1$, with a range of $0.89 \sim 1$ based on reported values [4, 10].

Mating We assumed equal male mating competitiveness between the infected and uninfected males [39] and further assumed a homogeneous mixing of males at a given location and time. Under these assumptions, the probability of a female mating with an uninfected male is given by $M_u/(M_u+M_w)$.

B.2 Estimate on diffusion coefficients

The diffusion coefficients for male and female mosquitoes are assumed to be the same, as their daily dispersion distances are not statistically different [49]. Consider the 2-D diffusion equation $u_t = D\Delta u (D>0)$ and its solution to the initial value problem:

$$u(\boldsymbol{x},t) = \int_{\mathbb{R}^2} \frac{1}{4\pi D t} e^{-\frac{|\boldsymbol{x}-\boldsymbol{y}|^2}{4Dt}} u(\boldsymbol{y},0) d\boldsymbol{y}, \ \boldsymbol{x} \in \mathbb{R}^2, \ t>0,$$

which can be rewritten as

$$u(\boldsymbol{x},t+\Delta t) = \int_{\mathbb{R}^2} k(\boldsymbol{x}-\boldsymbol{y},\Delta t) u(\boldsymbol{y},t) d\boldsymbol{y},$$

where

$$k(\boldsymbol{x},\Delta t) = \frac{1}{4\pi D\Delta t} e^{-\frac{|\boldsymbol{x}|^2}{4D\Delta t}} \sim \mathcal{N}_2\left(0, \begin{bmatrix} 2D\Delta t & 0 \\ 0 & 2D\Delta t \end{bmatrix}\right).$$

We assume mosquito dispersal per unit time Δt follows the heat kernel $k(\boldsymbol{x}, \Delta t)$ [23, 65], which is a two-dimensional Gaussian distribution with standard deviation $\sigma_{\Delta t} = \sqrt{2D\Delta t}$. To estimate the diffusion coefficient D, we match the mean absolute deviation (MAD) of the distribution, $E_{\Delta t} = \sigma_{\Delta t}\sqrt{\pi/2} = \sqrt{\pi D \Delta t}$, to the mean distance travelled (MDT) measured in biological studies [66].

We refer to two field studies in Australia: one in Pentland [49], a rural inland town with a drier climate, and another in Cairns [50], a coastal city with more humid weather. Both studies use the standard mark-release-recapture methodology. In the Pentland study, the daily MDT was estimated to be 25m/day. Using $E_1 = \sqrt{\pi D} = 25$, we calculate $D = 200$ m^2/day. Using the weekly MDT estimates of 60m/week, $E_7 = \sqrt{\pi D \times 7} = 60$, gives $D = 160$m^2/day.

In the Cairns study, daily MDT estimates were not available, but MDT values were reported at different time points, $E_5 = 70$ ($D \approx 310$), $E_8 = 55$ ($D \approx 120$), $E_{11} = 140$ ($D \approx 570$), $E_{15} = 100$ ($D \approx 210$), with the capture number decreasing in time. The overall MDT (within 15 days) was estimated to be $E_{15}^{all} = 78$ ($D \approx 130$). The lower MDT in Cairns compared to Pentland may reflect shorter flights in the humid environment, where mosquitoes are less pressured to seek distant oviposition sites.

Daily dispersal gives a more reliable characterisation of mosquito movement, as it is less likely to be affected by mosquito lifespan. Based on the Pentland data and MDT values from early time points in Cairns, we adopt $D = 200$ m^2/day as the baseline value. To capture the significant variability in the mosquito dispersal due to environmental and climatic factors [49], we use a broad range of $100 \sim 300$ m^2/day for D in our sensitivity analyses.

B.3 Incorporation of seasonality

We incorporate the impact of seasonality by introducing time-varying parameters for the mosquito life trait and carrying capacity K_l, which depends on the seasonal temperature (T) and rainfall (R). The governing equations are as follows:

$$
\begin{aligned}
(E_u)_t &= \phi_u(T)\frac{M_u}{M_u + M_w}F_u + (1-v_w)\phi_w(T)F_w - \delta(T)E_u - \mu_{eu}(T)E_u,\\
(E_w)_t &= v_w\phi_w(T)F_w - \delta(T)E_w - \mu_{ew}(T)E_w,\\
(L_u)_t &= \delta(T)E_u\left(1 - \frac{L_u + L_w}{K_l(R)}\right) - \psi(T)L_u - \mu_l(T)L_u,\\
(L_w)_t &= \delta(T)E_w\left(1 - \frac{L_u + L_w}{K_l(R)}\right) - \psi(T)L_w - \mu_l(T)L_w,\\
(F_u)_t &= b_f\psi(T)L_u - \mu_{fu}(T)F_u + D_1\Delta F_u,\\
(F_w)_t &= b_f\psi(T)L_w - \mu_{fw}(T)F_w + D_2\Delta F_w,\\
(M_u)_t &= b_m\psi(T)L_u - \mu_{mu}(T)M_u + D_3\Delta M_u,\\
(M_w)_t &= b_m\psi(T)L_w - \mu_{mw}(T)M_w + D_4\Delta M_w.
\end{aligned}
$$

The seasonal profiles for temperature and rainfall are presented in Appendix B.3.1, while the functional dependencies of parameters on these climate factors are detailed in Appendix B.3.2.

B.3.1 Climate profiles

We analyse climate profiles from two regions, Cairns, Australia, and Yogyakarta, Indonesia. For Cairns, data were obtained from the National Oceanic and Atmospheric Administration (NOAA)'s Climate Data Online [67], using records from the CAIRNS POST OFFICE, AS, weather station. The data include the average hourly temperature and precipitation for the city, which were aggregated into monthly measurements for curve fitting. For Indonesia, climate data were sourced from the Climate Change Knowledge Portal (CCKP) [68], using monthly average values over the period 1991 - 2022. We fitted periodic functions with a one-year period to the temperature and rainfall data using a non-linear least squares algorithm (`fminsearch` in MATLAB). The resulting fitted functions are given in Table B.1 and plotted in Fig B.2.

Table B.1: Fitted functions for seasonal climate profiles. The corresponding plots for temperature and rainfall are shown in Fig B.2. Carrying capacity, K_l, is rescaled from rainfall, R, as detailed in Appendix B.3.3.

	Cairns, Australia	Indonesia
Temperature (T)	$3.98\sin(2\pi t/365 + 0.20) + 24.78$	$-0.34\sin(2\pi 1.88(t/365 + 0.08)) + 25.93$
Rainfall (R)	$0.03((1.47\sin(2\pi(t/365 + 0.17)) + 1.47)^{2.54} + 1)$	$-0.07\sin(2\pi(t/365 + 0.67)) + 0.23$
Carrying capacity (K_l)	$0.06((1.47\sin(2\pi(t/365 + 0.17)) + 1.47)^{2.54} + 1)$	$-0.40\sin(2\pi(t/365 + 0.67)) + 1.40$

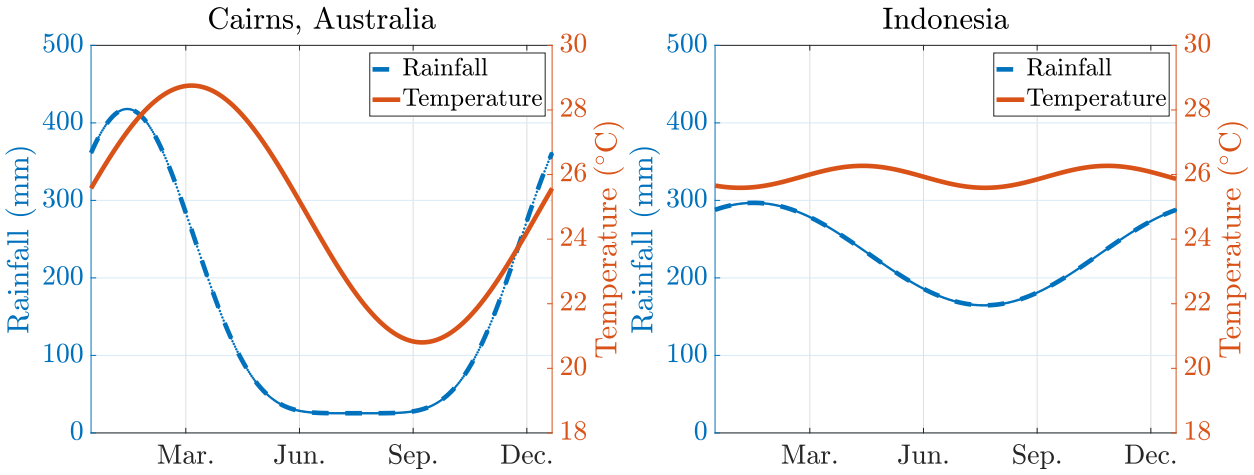

Fig B.2: Fitted seasonal rainfall and temperature curves for Cairns, Australia (left) and Yogyakarta, Indonesia (right). The corresponding fitted functions are provided in Table B.1.

B.3.2 Impact on mosquito life trait parameters

For mosquito life traits, we utilised temperature-dependent measurements from the literature [44, 69, 70] (top section of Table B.2). These quantities were transformed into the model parameters and rescaled to align with baseline estimates at 26°C (Table 1), the bottom section of Table B.2. The biologically relevant quantities are visualised in Fig B.3.

B.3.3 Impact on mosquito breeding sites

We incorporate the impact of seasonal rainfall variation into the carrying capacity, $K_l(R)$. More sophisticated implementations could also incorporate temperature dependence, as explored in studies such as [71, 72]. In particular, we rescaled the rainfall curves fitted in Appendix B.3.1 so that the maximum values match the baseline carrying capacity (one mosquito per square metre) for each rainfall function. The resulting functions are provided in Table B.1 (row 3).

Table B.2: Temperature dependence functions for mosquito life traits, transformed into model parameters and rescaled to match the baseline values in Table 1 at 26°C. † For each temperature dependence function $f(x)$, the actual value used is $\max\{f(x), 0\}$, to ensure positivity.

	Parameters	Temperature dependence†	Reference
$s_{P\to A}$	Pupae → adult trans. rate	$1.32\times10^{-9}T^8-2.49\times10^{-7}T^7+1.99\times10^{-5}T^6-8.80\times10^{-4}T^5+0.024T^4-0.39T^3+3.88T^2-21.33T+49.51$	[44]
μ_P	Pupae mortality rate	$4.40\times10^{-7}T^3+7.06\times10^{-4}T^2-0.033T+0.43$	[44]
μ_L	Larvae mortality rate	$7.503\times10^{-6}T^4-7.54\times10^{-4}T^3+2.74\times10^{-2}T^2-0.42T+2.32$	[44]
$s_{L\to P}$	Larvae → pupae trans. rate	$1.55\times10^{-9}T^7-2.62\times10^{-7}T^6+1.80\times10^{-5}T^5-6.46\times10^{-4}T^4+0.013T^3-0.15T^2+0.83T-1.85$	[44]
τ_F	Unadjusted female lifespan	$-0.11T^2+4.87T-26.25$	[69]
ϕ^*	Unadjusted female egg-laying rate	$0.01(T-14.58)T(34.61-T)^{0.51}$	[69]
δ^*	Unadjusted hatching rate for eggs	$6.43\times10^{-4}x(x-16)(35-x)^{0.34}$	[70]
μ_E	Unadjusted egg mortality rate	$1/\left(1.15\times10^{-4}x(x-12)(36-x)^{3.08}\right)$	[70]
	Transformed and rescaled parameters (used in the main text for seasonality results)		Baseline
ϕ_u	Egg-laying rate for uninf. females	$\phi^*\times0.5$	3.7
ϕ_w	Egg-laying rate for infected females	$\phi^*\times0.47$	3.5
δ	Hatching rate for eggs	$\delta^*\times1.41$	0.5
ψ	Larvae to adult develop. rate	$1/(1/s_{L\to P}+1/s_{P\to A})\times0.75$	0.1
μ_{eu}	Death rate for uninf. eggs	$\mu_E\times4.47$	0.088
μ_{ew}	Death rate for infected eggs	$\mu_E\times9.40$	0.185
μ_l	Death rates for larvae/pupae stages	$(\psi(s_{L\to P}+\mu_L)(s_{P\to A}+\mu_P)/(s_{L\to P}s_{P\to A})-\psi)\times1.35$	0.12
μ_{fu}	Death rate for uninf. females	$1/\tau_F\times1.59$	1/17.5
μ_{fw}	Death rate for infected females	$1/\tau_F\times1.76$	1/15.8
μ_{mu}	Death rate for uninf. males	$1/\tau_F\times2.64$	1/10.5
μ_{mw}	Death rate for infected males	$1/\tau_F\times2.64$	1/10.5

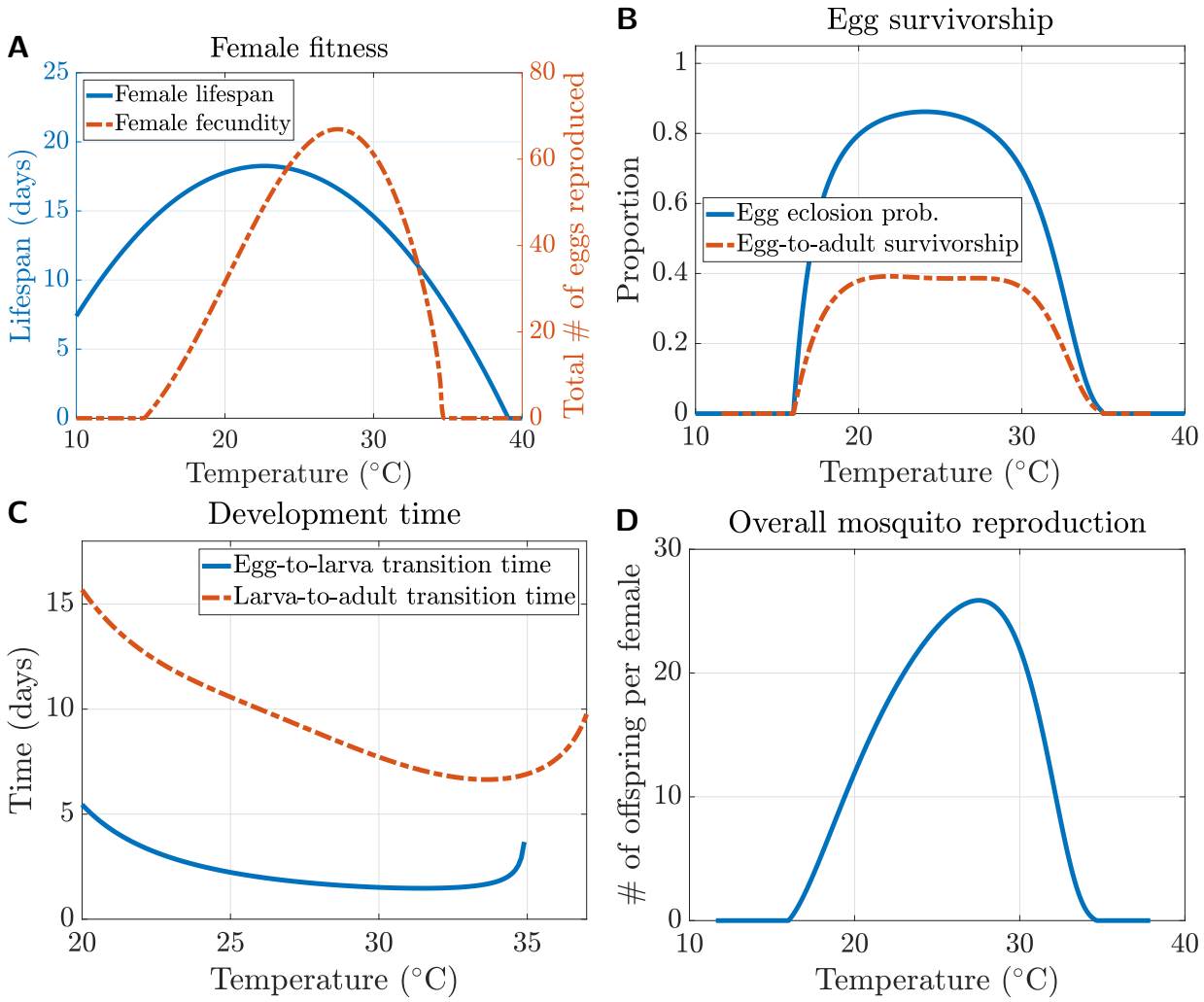

Fig B.3: Temperature-dependent mosquito life traits. (A) Female fitness: lifespan in days ($1/\mu_{fu}$) and number of eggs reproduced per female (ϕ_u/μ_{fu}). (B) Egg survivorship: proportion of eggs that eclose ($\frac{\delta}{\delta+\mu_{eu}}$), and proportion of eggs surviving to adulthood ($\frac{\delta\psi}{(\delta+\mu_{eu})(\psi+\mu_l)}$). (C) The development time for juvenile stages: egg-to-larva transition time ($1/\delta$) and larva-to-adult transition time ($1/\psi$). (D) Overall mosquito reproduction, defined as the number of offspring that survive to adulthood per female mosquito: $\frac{\phi_u}{\mu_{fu}}\frac{\delta\psi}{(\delta+\mu_{eu})(\psi+\mu_l)}$.

C Details on sensitivity analysis

Below we provide details on the quantities of interest (QOIs) and the sampling methods for the sensitivity analysis in Section 3.1 of the main text. For PRCC results, we confirmed that all QOIs satisfy the monotonicity requirement.

C.1 Quantities of interest

Critical bubble quantities: For quantities related to the critical bubble, we define the fraction of infection in female mosquitoes as:

$$p^*(x,y) = \frac{F_w^*(x,y)}{F_u^*(x,y) + F_w^*(x,y)},$$

where F_u^* and F_w^* are the solutions of the uninfected and infected female populations, respectively, of the critical bubble. The infection profile is illustrated in Fig C.4A.

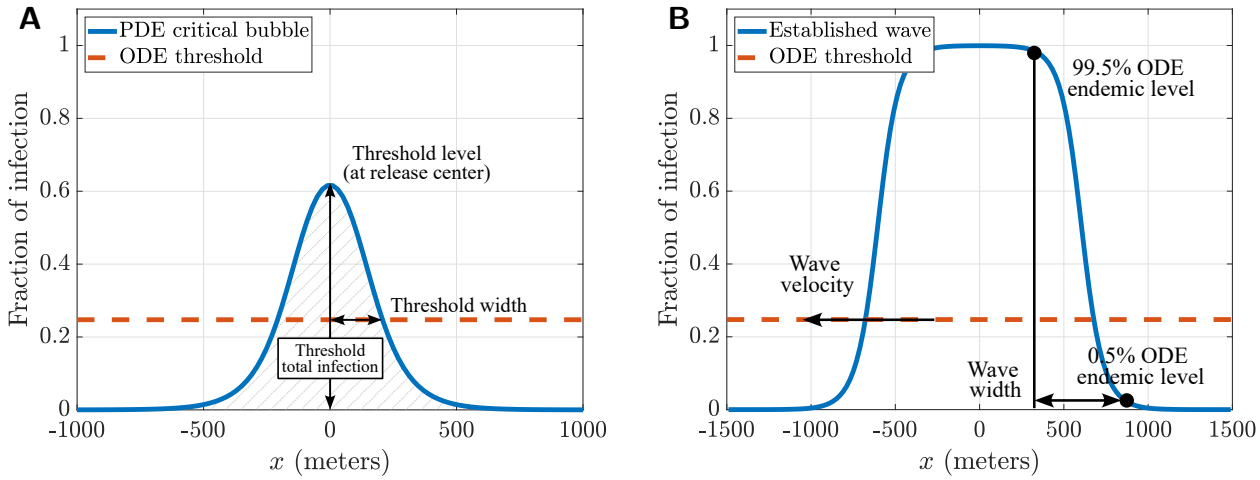

Fig C.4: Quantities for sensitivity analysis. (A) Threshold-related quantities, including the threshold level, threshold width, and threshold total infection (the shaded area under the curve). (B) Wave-related quantities, including wave velocity (assuming outward propagation) and wave width.

1. Threshold total infection: This measures the overall fraction of infection within the bubble's coverage, $\Omega \in \mathbb{R}^2$:

$$\text{QOI} = \int_\Omega p^*(x,y)dxdy$$

2. Threshold level: The fraction of infection at the release centre of the critical bubble, $\text{QOI} = p^*(0,0)$.

3. Threshold width: This measures the spread of the critical bubble. It is calculated as the radial distance from the release centre, (0, 0), to the inflection point of the bubble front (Fig C.4A). At the inflection point, the fraction of infection matches the ODE threshold level p_{ODE}, derived in [38],

$$p_{ODE} = \frac{r_{wu}\frac{1}{\mu_{fw}}}{\frac{1}{\mu_{fu}} + r_{wu}\frac{1}{\mu_{fw}}}, \tag{C.1}$$

where r_{wu} is the smaller root for the following equation

$$\frac{v_u}{v_w}\frac{\delta+\mu_{ew}}{\delta+\mu_{eu}}r_{wu}^2 + \left(\frac{v_u}{v_w}\frac{\delta+\mu_{ew}}{\delta+\mu_{eu}} - 1\right)r_{wu} + \frac{1-\mathcal{R}_0}{\mathcal{R}_0} = 0, \tag{C.2}$$

and $\mathcal{R}_0$ is the basic reproduction number as defined in Eq. (1) in the main text. Due to the radial symmetry of the bubble, there are infinitely many inflection points located on a circle. For simplicity, we select the point on the positive x-axis, that is, $p^*(x_{inf}, 0)$ and define the threshold width $\text{QOI} = x_{inf}$.

Infection wave quantities: For the infection wave, we consider the fraction of infection in female mosquitoes at a large final time, when an asymptotic propagating wave has formed:

$$p^{**}(x,y) = \frac{F_w^{**}(x,y)}{F_u^{**}(x,y) + F_w^{**}(x,y)}.$$

The solution is a smooth transition front connecting two stable ODE steady states (Fig C.4B).

1. Wave velocity: This is the velocity of wave propagation (assuming expanding coverage, $c > 0$, and radial symmetry):

$$c(x_{inf}) \approx \frac{-p_t^{**}(x_{inf},0)}{p_x^{**}(x_{inf},0)},$$

   where x_{inf} is the inflection point calculated as in the threshold width, p_t is evaluated based on the right-hand side of the equations, and p_x is approximated using numerical derivatives. We use the asymptotic wave velocity as a proxy and define wave velocity as QOI $= c(x_{inf})$.

2. Wave width: This measures how spread out the wavefront is, calculated as the horizontal distance between 99.5% of the ODE endemic infection rate and 0.5% infection (Fig C.4B). The ODE endemic infection level is determined using Eq. (C.1), where r_{wu} is the larger root of Eq. (C.2). Further details on ODE steady states can be found in [38].

C.2 Parameter samplings

When implementing the global sensitivity analysis, we adjusted the parameter ranges so that all parameters of interest (POIs) are varied by a comparable relative amount. The updated parameter ranges are listed in Table C.3.

To ensure biological relevancy, we enforced the following assumptions across all samples: a reduced reproduction rate for *Wolbachia*-infected females ($\phi_w < \phi_u$), increased death rates for infected females ($\mu_{fw} > \mu_{fu}$) and infected eggs ($\mu_{ew} > \mu_{eu}$). To incorporate these fitness costs, we introduce the independent fitness cost parameters (e.g. c_ϕ) as the POIs for sampling. The dependent parameters are then back-calculated (e.g. $\phi_w = \phi_u(1 - c_\phi)$).

Additionally, we maintain the model assumptions that *Wolbachia* infection does not impact male death rates ($\mu_{mw} = \mu_{mu}$) or mosquito dispersal ($D_1 = D_3$, $D_2 = D_4$). As a result, μ_{mu}, D_1, and D_3 were treated as independent POIs.

Table C.3: Model parameters involved in the sensitivity analysis (SA) and their baseline values. All the rates have dimension day^{-1} and are estimated based on the wMel strain of *Wolbachia* and *Aedes aegypti* mosquitoes, see Table 1. The ranges for SA have been adjusted to $[0.75X, 1.25X]$, where X is the baseline value, subject to biological constraints. § indicates new fitness cost parameters for sampling purposes.

Parameters		Baseline	Range for SA	Reference	Notes
ϕ_u	Per capita egg-laying rate for F_u	3.7	$2.775 \sim 4.625$	[10, 43, 44]	
c_ϕ	Fitness cost: reduction in egg-laying rates§	0.054	$0.041 \sim 0.068$	[10, 43]	$\phi_w = \phi_u(1 - c_\phi)$
δ	Per capita hatching rate for eggs	0.5	$0.375 \sim 0.625$	[45, 46]	
ψ	Per capita development rate	0.1	$0.075 \sim 0.125$	[4, 46]	
μ_{eu}	Death rate for E_u	0.088	$0.066 \sim 0.11$	[10, 45]	
$c_{\mu e}$	Fitness cost: increase in egg death rates§	1.102	$0.827 \sim 1.378$	[10, 45]	$\mu_{ew} = \mu_{eu}(1 + c_{\mu e})$
μ_l	Death rate for L_u and L_w	0.12	$0.09 \sim 0.15$	[44]	
μ_{fu}	Death rate for F_u	1/17.5	$1/23.33 \sim 1/14$	[19, 47, 48]	
$c_{\mu f}$	Fitness cost: increase in female death rates§	0.108	$0.081 \sim 0.135$	[4]	$\mu_{fw} = \mu_{fu}(1 + c_{\mu f})$
μ_{mu}	Death rate for M_u	1/10.5	$1/14 \sim 1/8.4$	[43]	$\mu_{mw} = \mu_{mu}$
v_w	Maternal transmission rate	1	$0.89 \sim 1$	[4, 10]	biological constraint
D_1	Diffusion coefficients (m^2/day)	200	$150 \sim 250$	[23, 49, 50]	$D_1 = D_2 = D_3 = D_4$

D Additional plots for results

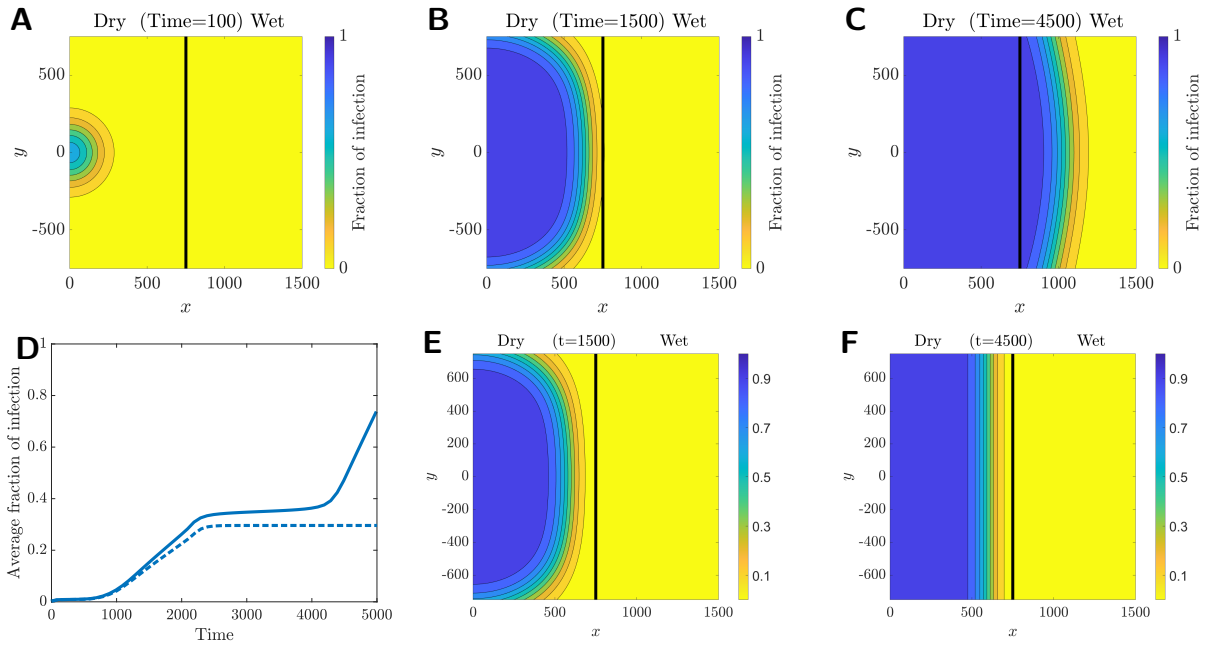

Fig D.5: Release infection in the dry vs. wet regions. (A)–(C) Results for a dry-to-wet carrying capacity ratio of 1 : 2.5. (E)–(F) Results for a dry-to-wet carrying capacity ratio of 1 : 5. (D) The average fraction of infection across the entire domain for both scenarios: solid curve for the 1 : 2.5 ratio and dashed curve for the 1 : 5 ratio, where the infection wave stops near the dry-wet interface.

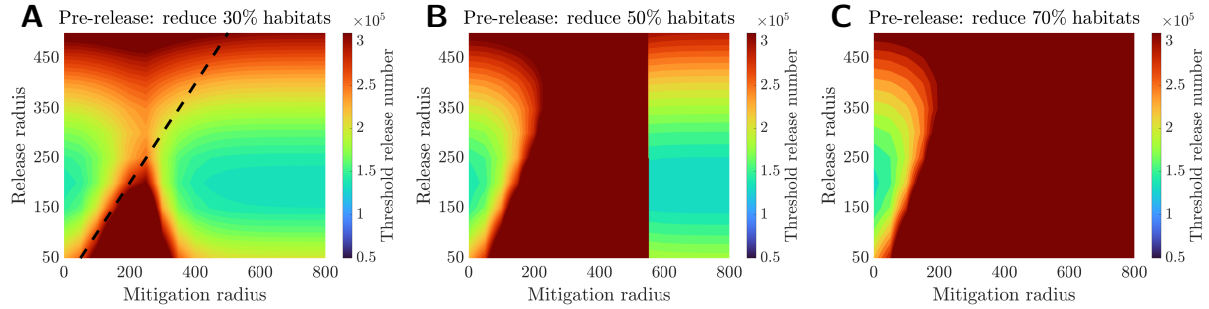

Fig D.6: Pre-release mitigation through habitat modifications, removing (A) 30% (same as Fig 5G), (B) 50%, and (C) 70% of the breeding sites. Regions with a threshold release number exceeding 3×10^5 are shown in dark red and are considered non-achievable. As the reduction fraction increases, the non-achievable regions expand.